

Article

Simulation and Test Bed of a Low-Power Digital Excitation System for Industry 4.0

Jun-Ho Huh ¹ and Hoon-Gi Lee ^{2,3,*}

¹ Department of Software, Catholic University of Pusan, Busan 46252, Korea; 72networks@pukyong.ac.kr or 72networks@cup.ac.kr

² System Development Division of E2S, Seoul 05307, Korea

³ Department of Electrical and Computer Engineering, University of Seoul, Seoul 02504, Korea

* Correspondence: hglee@e2s.co.kr or hoongi.lee@gmail.com

Received: 18 July 2018; Accepted: 25 August 2018; Published: 1 September 2018



Abstract: Since modeling and simulation are the two most effective tools that can be used in the design or analysis process, they play a vital role in developing such system. In many cases, they are the only possible means of making a safe engineering decision for a new concept of process for a large-scale system. Elsewhere, they are used as a critical element in the analysis of energy systems or to suggest a method of developing a novel and effective energy system model. Thus, in this study, simulations and test bed experiment were carried out to assess a low-power digital excitation system in order to validate its effectiveness. The excitation systems currently used by most of the power stations in the Republic of Korea were installed during the 1970s or 1980s. Unfortunately, it is difficult to seek technical assistance for them as they depend on foreign technologies, requiring a large sum to be paid when requesting one or more engineers to be dispatched. As such, technical updates have always been made by foreign companies, since it is not easy to make modifications to the system without the help of the original system developer. The technology developed in this study was designed to address such problem. The inability to conduct a test for an actual system can be solved by using a power system analysis program to analyze the characteristics of the controller. The study confirmed the system's effectiveness, and the Test Bed was proven to be flexible and adequate for the experiment. The proposed excitation system is expected to increase the stability and economic effect of the system by optimizing existing systems. In the future, the authors plan to focus on student education by establishing an education system that allows students to learn about the digital excitation system and its simulation.

Keywords: simulation; Test Bed; low power; digital excitation system; Industry 4.0; computer architecture; operating system; smart grid

1. Introduction

From an economic standpoint, some of the most important elements are the production, management, and consumption of energy or energy products. These are basically associated with many other critical social elements such as food production, water consumption, manufacturing, resource management, security, and environment. Currently, process system engineering is in a position where it can solve the most important problems associated with energy systems and mitigate their impact on all countries around the world [1–3].

The explosive increase in power consumption has largely affected the supply and demand for energy, causing rapid changes in the energy market. Such changes are leading to a steady increase in the capacity of power-generating units in the Republic of Korea (ROK). Excitation systems, which play a vital role in recovering power generation systems or dealing with sudden and unexpected changes

in voltage, should be installed in all units, and especially in small or medium-sized generators or synchronous motors [4–7].

The equipment run by a system that adjusts the DC (Direct Current) current of a field coil to control the output voltage of a generator is important due to its effectiveness in improving the quality of electricity and stabilizing the power system. The equipment relies on its technical stabilization and reliability, significantly affects the users of electricity including industry and the public, and requires advanced techniques related to the power system. After discussions about the problems that occur during the operation of the digital excitation system as well as all the types of generators, equipment protection and accident prevention have been made possible.

An excitation system maintains or controls the output terminal voltage by supplying direct current to the field winding; it is essential not only to power plants but also to the smart factories of the 4th Industrial Revolution. In other words, it is part of the internal system of an emergency diesel generator, generating voltage for the generator and supplying constant current to various types of equipment uniformly. As a core piece of equipment that supplies power to the cooling pump or cooling fan necessary for the cooling of nuclear reactors or other power-generating facilities, the emergency diesel generator is activated as soon as these facilities stop. The excitation system assumes the role of assisting the emergency diesel generator in maintaining constant voltage and running properly by comprehensively controlling the current. It automatically kicks in when the nuclear reactor or power generation facility stops operating and restores power within the power plant within 10 s. Even if the voltage of the emergency diesel generator drops suddenly, the system will restore it to the original level. Ultimately, the excitation system is a core piece of equipment that allows the emergency diesel generator, cooling facility, or nuclear reactor to work properly in an emergency that causes failure.

Although the Triple Modular Redundant (TMR) excitation system developed in the Republic of Korea is now operating commercially at a 1000 MW-class nuclear power plant, installing such large excitation systems can be very costly as they are normally designed and developed for large-scale power plants. For this reason, the TMR excitation system is considered unsuitable for small-scale power plants or industrial power plants where small/medium-sized generators are operating [7–10]. Thus, simulations and Test Bed experiment were conducted on the proposed low-power digital excitation system.

If a test is conducted by simulating an accident of a certain power plant's digital excitation system directly at the operating site, problems could occur at the plant or in the power system. This study aims at the smooth operation of the entire system with the support of a protective relay and through simulation of the excitation system's integrity and system stability. It was difficult to maintain as it was made in the US, and problems would occur in the power plant's power system if the simulation test for the excitation system is conducted at the actual sites; hence the need for a test bed or a simulation model. As such, an attempt was made to achieve the smooth running operation of the excitation system by testing its integrity and the power system's stability through simulations in combination with the protective relay.

As part of the equipment, the digital excitation system controls the output voltage of a generator by managing the level of direct current flowing in the field winding of a synchronous generator. It is a primary piece of equipment that affects the stabilization of a power system and the improvement of power quality. The major elements of such system include the Automatic Voltage Regulator (AVR), Manual Voltage Regulator (MVR), Over Excitation Limiter (OEL), Under Excitation Limiter (UEL), V/Hz limiter, over excitation protection, overvoltage protection, and PT (Potential Transformer)-failure scanning. These elements were subjected to a PSIM (Powersim inc.) simulation along with a Test Bed experiment of the proposed method.

The rest of this paper is organized as follows: Section 2 introduces Related Studies; Section 3 describes the Operation Test of the Proposed Digital Excitation System with the Task Program Using u/C OS (Operating System), with the Configuration of Redundant Controller and Startup Test,

ETAP (Electrical Transient Analyzer Program) Simulation, and Performance Evaluation detailed in Sections 4–6, respectively; the Conclusion is presented in Section 7.

2. Related Research

Among the research studies conducted on excitation systems in the Republic of Korea, Ho-Sun Ryu developed a static excitation system that has both main and sub-controllers for the No. 4 generator unit at the Incheon Thermolectric Power Plant [11]. On the other hand, Gyeon-Cheol Kim conducted research on the development of a redundant digital excitation system and its application [12]. Meanwhile, Chae-Ho Nam designed and implemented a redundant digital excitation system for power plants [13]. The software architecture of this system is programmed based on a real-time operating system as shown in Figure 1. The system itself consists of a real-time operating system kernel and a library, a Board Support Package (BSP) for the MV2306 Motorola CPU (Central Processing Unit) board embedded with a PowerPC (MPC604) CPU, a device driver for every kind of I/O board, and an application program for excitation control [13].

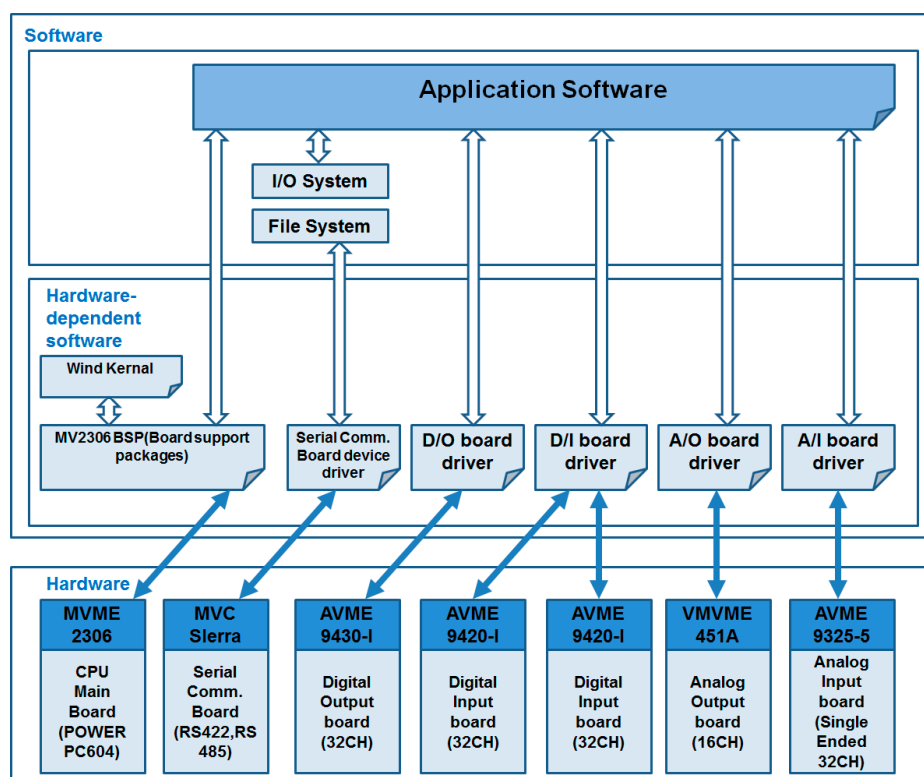


Figure 1. Architecture of the Digital Excitation System.

Ho-Sun Ryu also conducted research on the digital excitation system installed at a pumped storage power plant [14]. Meanwhile, Jea-Do Lee performed an analysis of a digital excitation system consisting of IGBTs (Insulated Gate Bipolar Transistors) [15]. Soo-Jin Jang studied an excitation system for synchronous generators using a current-control PWM (Pulse Width Modulation) converter, whereas Ho-Sun Ryu worked on a simulator for static digital excitation systems [16,17]. Man-Soo Shin developed control and diagnosis techniques for excitation systems, with Ho-Sun Ryu developing a redundant excitation system for the thermolectric power station in Khartoum, Sudan [18,19]. In addition, Juhyun Lee developed and applied a redundant digital excitation system for nuclear power stations, whereas Ho-sun Ryu conducted research on a digital excitation system by adopting a regenerative redundant PWM (Pulse Width Modulation) method. Figure 2 shows a model of a static excitation system receiving power directly from the generator output terminal [20,21].

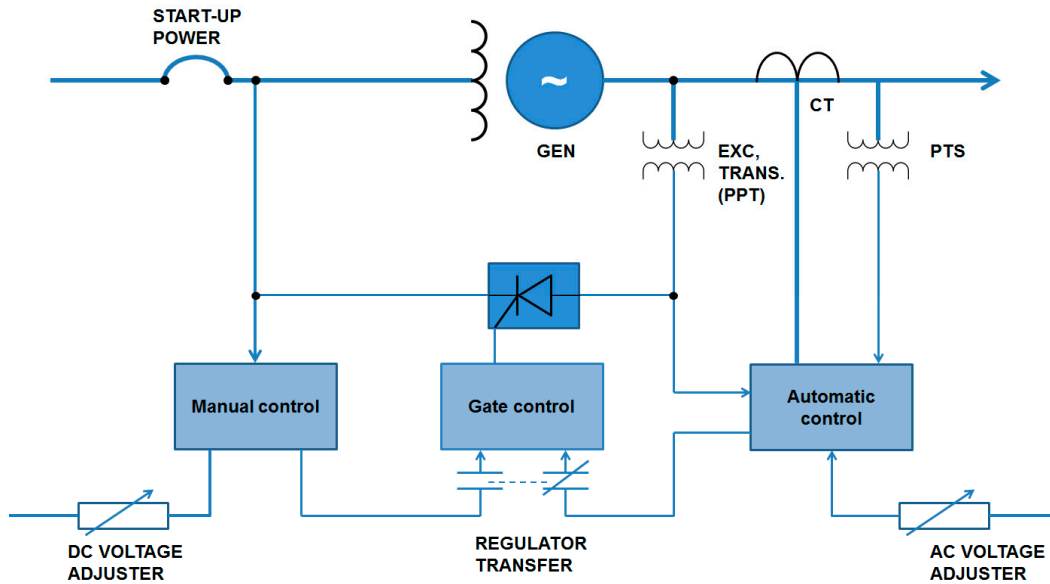


Figure 2. Static Digital Excitation System Model.

Soo-Hwan Jin tested the dynamic stability of a digital excitation system's thyristor, and Ho-Sun Ryu conducted research involving the functional testing of a simulator-mounted digital excitation system. More recently, his work has been applied to a 500 W synchronous generator.

Figure 3 shows the configuration of a simulator-mounted redundant digital excitation system. A triple redundant controller (Invensys) was used as the main controller, and a triple redundant signal processing board was also manufactured. A program for high-speed signal processing/calculation and power system stabilization equipment was embedded [22–24].

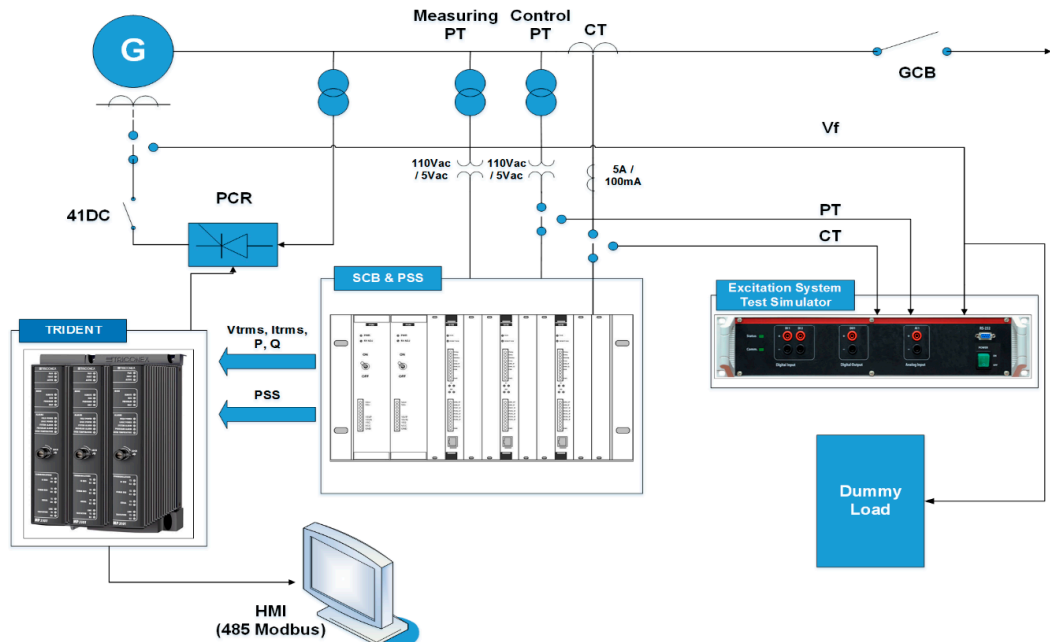


Figure 3. Simulator-Mounted Redundant Digital Excitation System.

Karel Maslo conducted research on the simplification and integration of an IEEE (Institute of Electrical and Electronics Engineers) standard model for excitation systems [25], whereas Hassan Yousef studied the control of a non-linear power system using an adaptive phablet network [26].

Jiawei Yang conducted research involving the analysis and evaluation of a VSC (Voltage Source Converter) excitation system in a bid to improve the stability of power systems [27], with M. Aldeen researching on the detection, identification, and mitigation of failures of distributed excitation systems [28]. A block diagram of a common excitation system is shown in Figure 4 below.

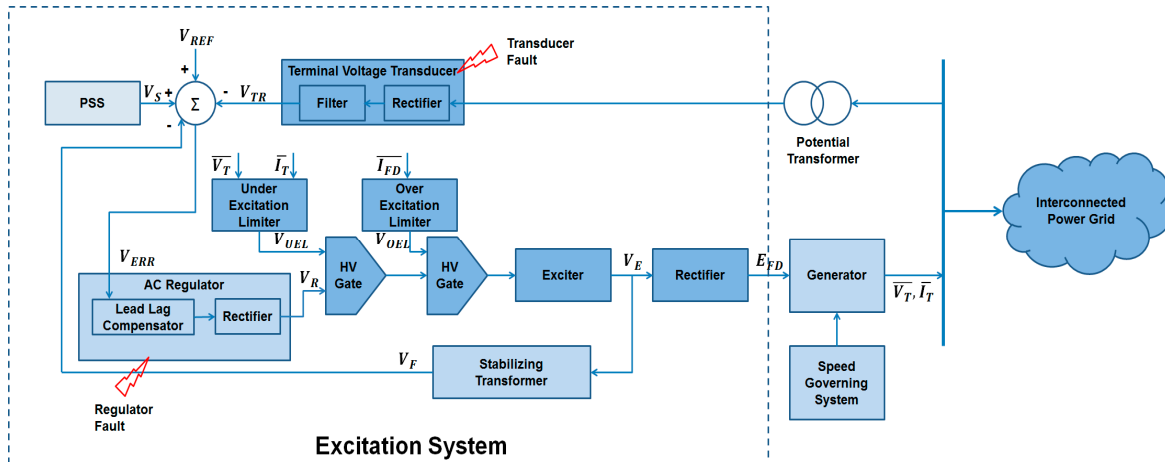


Figure 4. Block Diagram of a Common Excitation System.

Hong Zhang conducted research on the application of a non-linear PID (Proportional Integral Derivative) controller for a generator excitation system [29]. A. J. Saaverdra-Montez studied an identification technique for a generator excitation system staying online, along with a parameter estimation methodology based on experimental conditions [30,31]. Amin Khodabakhshian studied a cooperative design of STATCOM and excitation system controller of a redundant power system using a zero-dynamic technique [32]. Stephan M. Benchluch investigated a trajectory sensitivity estimation technique to identify the linear excitation system models [33]. Walmir Freitas and J. D. Hurley conducted research on the effects of excitation system control modes on the allowable level of penetration of distributed synchronous generators [34] and the negative effect of reactive power and power factor controller on excitation systems [35], respectively. Jing Shi investigated the excitation system of the SMES (Superconducting Magnetic Energy Storage)-based redundant inductive generator in the field of wind power generation [36]. X.C. Zhang studied user-defined excitation system models in order to analyze the stability of high-speed rectifier excitation systems [37], whereas Paul L. Dandeno conducted research on the effect of high-speed rectifier excitation systems on the stability limit of generators [38]. Dan Wang investigated the cooperative control between the EPT and a generator excitation system for a multi-layer circuit power transmission line system [39,40]. Similar to some of the power plants in the Republic of Korea, the technological dependence of power plants constructed more than 10 years ago is quite high, compared to those constructed in the US or EU, where their own technologies are being used. Especially, foreign-made excitation systems require highly skilled technical support and high costs for maintenance, which is sometimes not easily provided by the original developers.

The latest global trend of research on digital excitation systems is focused on the construction of dual-controller systems. Conventional generators use an analog excitation system. Therefore, the dual-system model proposed in this paper adopts a backup concept consisting of two controllers, which means that one controller is operated if the other one breaks down, thus avoiding problems with operating the generator.

Thus, it is necessary to change this situation by developing our own system that foregoes any reliance. In that regard, the simulation model proposed in this study will be able to provide an experimental methodology by which power plants can know what to expect when their new ideas

or inventions have been reflected to the present system. If the simulation result validates them, their upgrades will be justified.

3. Operation Test of the Proposed Digital Excitation System with a Task Program Using u/C OS

The power plants being referred to in this section are the critical facilities of the Republic of Korea, adopting a digital excitation system as most of the major factories do to achieve a high level of reliability. By using u/C OS, runtime scheduling becomes possible, and all the necessary functions can be combined for processing.

In this section, a task program developed for the digital excitation system was used to measure the operating time. Figure 5 shows the measurements of the operating times of the excitation control programs. An oscilloscope was used to measure the operating times of each control program. Meanwhile, the DSP (Digital Signal Process) and the RTOS (Real-Time Operating System)-mounted controller performed calculations by sampling the data such as rms, and P and Q frequencies at 1800 Hz after receiving the analog signal values, including the generator voltage and current, along with the field voltage and current.

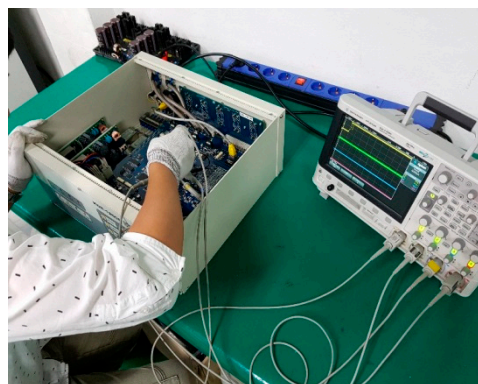


Figure 5. Operating Times of the Digital Excitation System with Task Program.

Using the preemptive multitasking function provided in the u/C OS, the tasks were separated after being categorized into independent task and dependent task by grouping the necessary functions based on their associations with each other. Each task was to perform a role by preemptively occupying the CPU depending on its importance. In other words, while there could be a task that should be performed periodically, there would also be a task that needed to be performed only when the environment has changed. These 4 tasks run on different frequencies using their own functions independently. The control section can be largely divided into automatic control and manual control. The AVR (Auto Voltage Regulator) and the UEL (Under Excitation Limiter) are automatically controlled at 180 Hz, whereas the FCR (Field Current Regulator) and the OEL (Over Excitation Limiter) are manually controlled at 360 Hz. The control system has been designed in such a way that the control signals are transmitted within the 6-pulse cycle ($60 \text{ Hz} \times 6 = 360 \text{ Hz}$) of the phase-controlled rectifier. The controller computes the RMS, P.Q, and frequency after receiving the analog signals of generator voltages/currents along with the field voltage/current data and sampling them at 1800 Hz using a DSP-embedded RTOS.

Meanwhile, the tasks were divided into independent or dependent tasks by combining the relevant necessary functions with the preemptive multitasking function provided by the u/C OS. Each task was to perform a role by preemptively occupying the CPU depending on its degree of importance. In other words, some are performed periodically, but others are performed only when the environment has changed. These four tasks operate at different frequencies and perform each function autonomously. The control part was largely divided into automatic control and manual control. For the former, an AVR (Auto Voltage Regulator) and a UEL (Under Excitation Limiter) were controlled at

180 Hz; for the latter, however, an FCR (Field Current Regulator) and an OEL (Over Excitation Limiter) operated under a control loop at 360 Hz. This allowed for the control signals to transmit within the 6-pulse signal cycle ($60 \text{ Hz} \times 6 = 360 \text{ Hz}$) of the phase-controlled rectifier.

Figure 6 shows the measurement of the operating time of the code that samples generator voltage/current and field voltage/current. The sampling cycle of ADC (Analog-Digital Converter) was 1.8 kHz, and the operating time was 20.833 kHz sec.

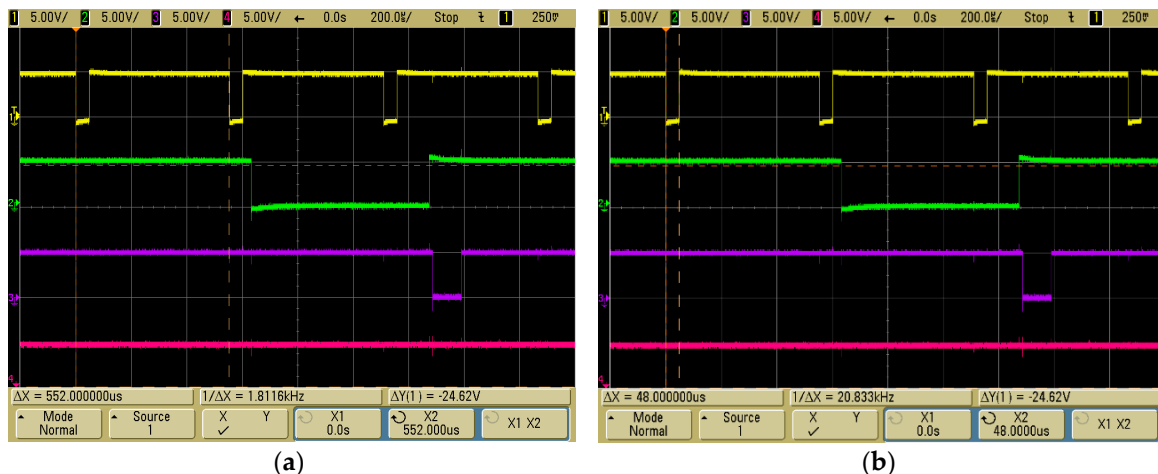


Figure 6. Measurement of Excitation Control Program Operating Time ADC (Analog-Digital Converter). (a) ADC-based Sampling Cycle; (b) ADC-based Sampling Time.

Figure 7 shows the operating time of the generator voltage and the current computed with DFT (Discrete Fourier Transform) with sampling cycle of 2.78 ms and operating time of 640 μs .

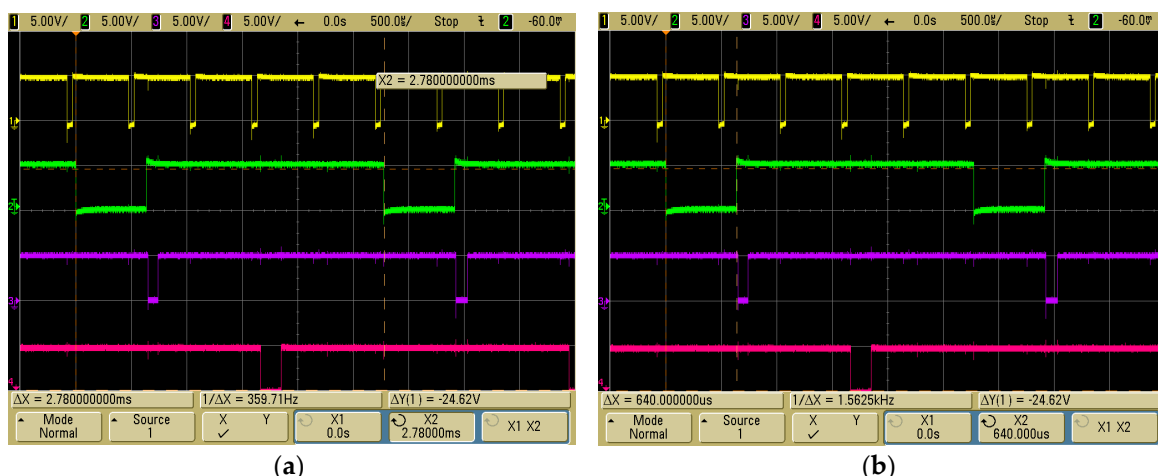


Figure 7. DFT (Discrete Fourier Transform)—based Measurement of the Excitation Control Program. (a) DFT-based Sampling Cycle; (b) DFT-based Sampling Time.

Figure 8 shows the operating time of the control program measured with the Task program. The sampling cycle was 2.77 ms, and the operating time was 92 μs .

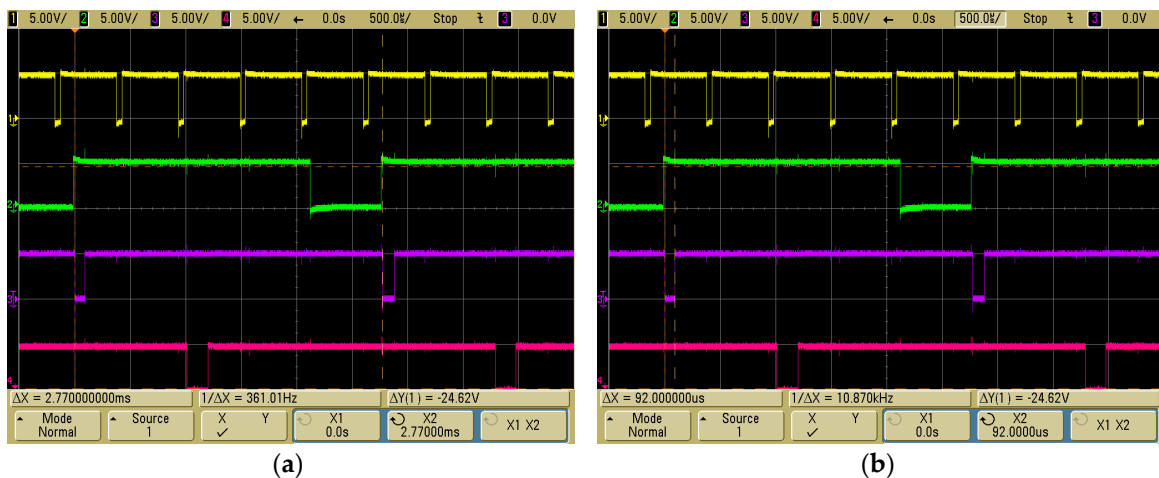


Figure 8. Measurement of the Excitation Control Program Operation (Task). (a) Control Sampling Cycle (Task); (b) Control Sampling Time (Task).

Figure 9 shows the operating time of the protection program measured with the Task program. The sampling cycle was 2.77 ms, and the operating time was 190 μ s. Figure 10 also presents the total operating time of the programs with sampling cycle of 1.85 ms.

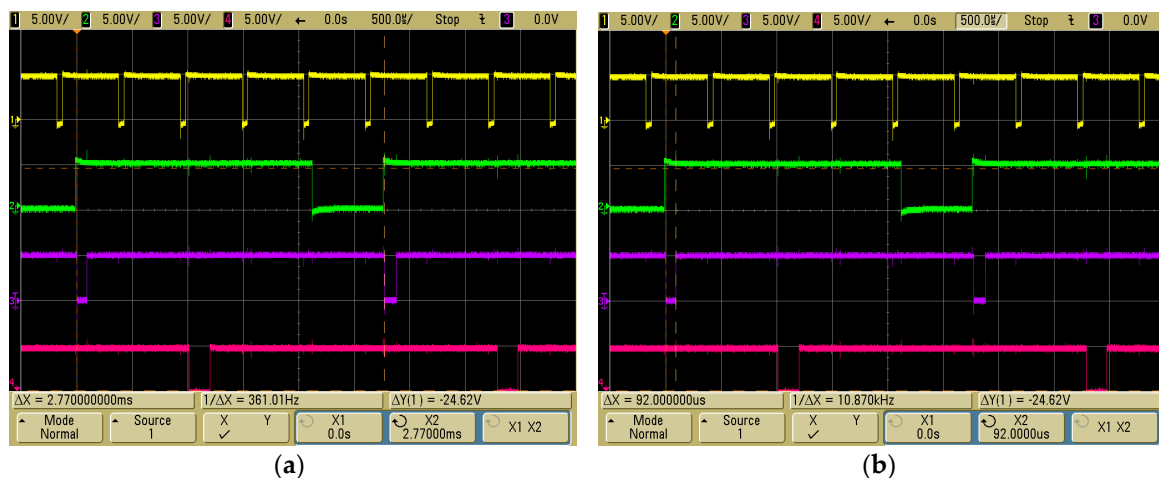


Figure 9. Measurement of the Excitation Protection Program Operation (Task). **(a)** Protection Program Sampling Cycle (Task); **(b)** Protection Program Sampling Time (Task).

For the simulation related to the operating time, the control section is largely divided into automatic control and manual control (Figures 6–10). In this simulation, the AVR (Auto Voltage Regulator) and the UEL (Under Excitation Limiter) are automatically controlled at 180 Hz, whereas the FCR (Field Current Regulator) and the OEL (Over Excitation Limiter) are manually controlled at 360 Hz, respectively. The control system has been designed in such a way that the control signals are transmitted within the 6-pulse cycle ($60 \text{ Hz} \times 6 = 360 \text{ Hz}$) of the phase-controlled rectifier. This was necessary to check the integrity of the controller by confirming that the control loop is operating normally. The simulation result showed that the controller was operating flawlessly.

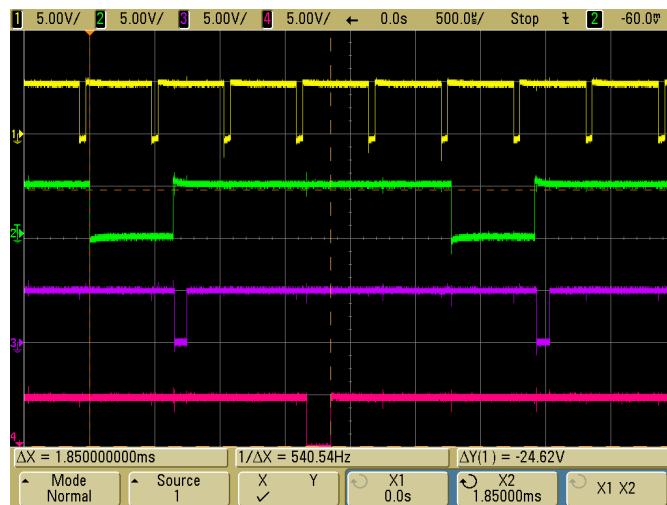


Figure 10. Total Operating Time of the Programs.

4. Configuration of Redundant Controller and Startup Test

In this section, the system has been configured in such a way that the operation will be quickly switched over to another controller when its primary controller becomes impossible to operate, in order to resume normal operation at the power plant. It is often impossible to repair or replace the digital excitation system immediately unless there is a reserve. To avoid such problem and resume normal operation, a redundant design is being applied to the system in order to address the problem of controller shutdown.

The controller is connected with a relay logic board to transmit a switchover output signal after checking for any abnormal operation or functional failure in the digital excitation controller. Figure 11 describes the configuration of the switchover circuit of the redundant controller. Each controller is embedded with a watchdog timer to generate pulse signals periodically. If these signals are not detected, the control function will be judged to have failed, and a switchover signal will be transmitted. Such test was performed since making the controller redundant allows the selected controller to operate first and makes another controller run if any problem occurs on either the human or the controller's side. The following are the conditions for using the manual mode: first, when the operator has decided to use the manual mode; second, when the controller is unable to detect the generator voltage; and finally, when there are problems in the transformer due to overvoltage or other failures. In these cases, the operator is required to monitor the system continually and make adjustments based on how the situation develops. In other words, the main objective is to maintain a constant system voltage with the excitation system.

A redundant switchover circuit was implemented as shown in Figure 12. Periodic pulse signals are generated using the DSP and FPGA (Field-Programmable Gate Array) of the controller; if the signals are not detected within a certain time limit, D-Flip-Flop-type switchover signals will be generated.

Figure 13 shows the order of the operation mode to be initiated when abnormalities are detected in the two controllers. The initial digital excitation control system is operated in "Auto" mode with Controller 1. Especially, they follow and watch the major control signals of each other in order to minimize excessive responses generated during the redundant switchover. If Controller 1 fails, a switchover to Controller 2 will be carried out to exchange the role of the main controller, maintaining "Auto" mode. When "Manual" mode is selected by the user or due to generator voltage loss during operation under Controller 2, the operating mode of Controller 2 will shift to manual. When an abnormality such as PT loss occurs during Controller 1 operation, however, the switchover will not occur, and the controller will maintain the manual operating mode.

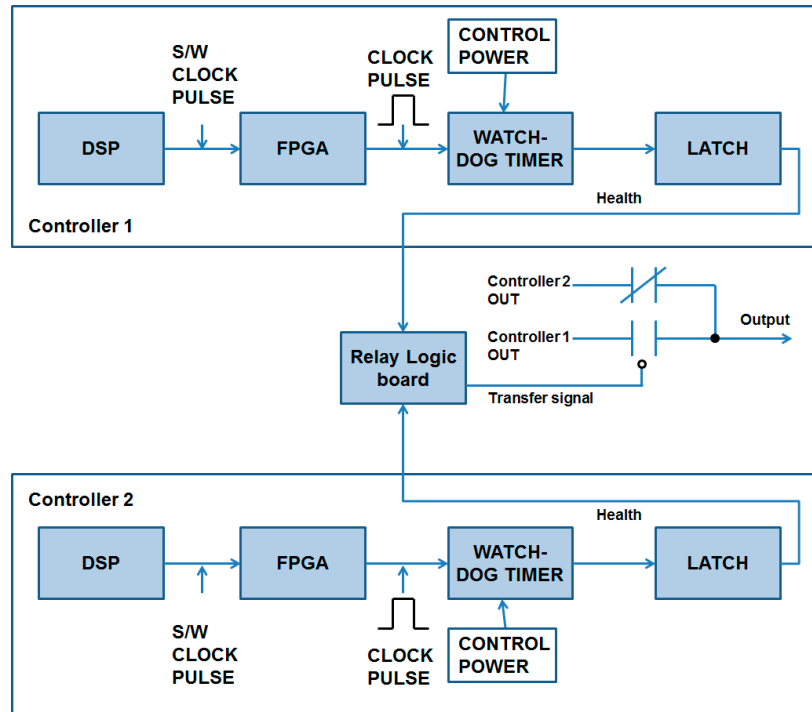


Figure 11. Configuration of the Switchover Circuit of the Redundant Controller.

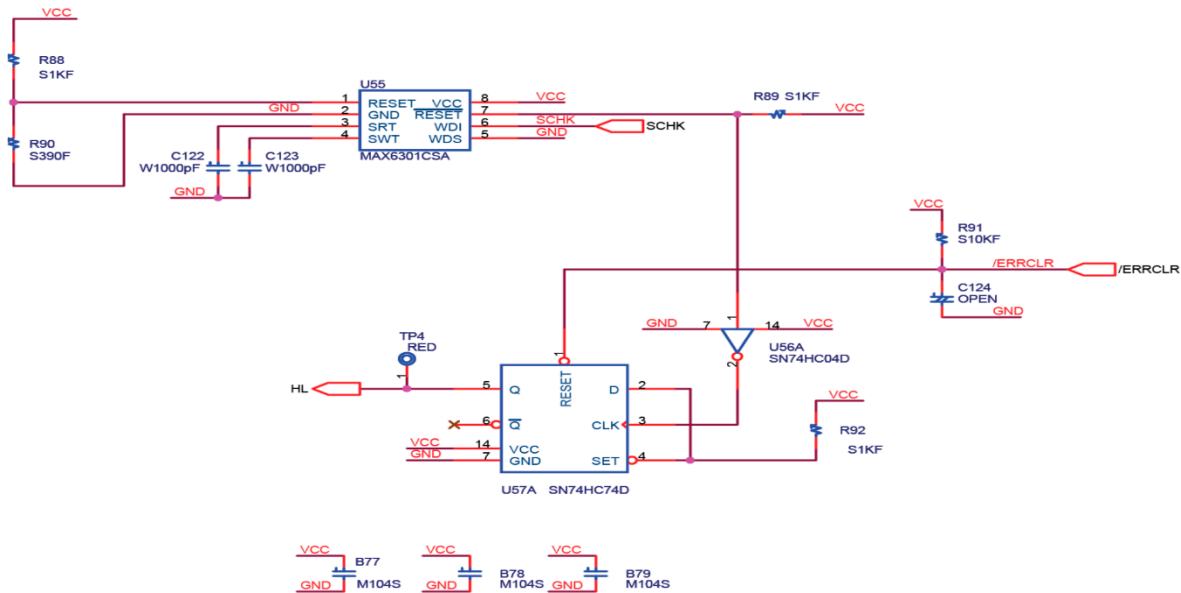


Figure 12. Redundant Controller Switchover Circuit.

On the other hand, both ABB (Zurich, Switzerland) and BASLER (Ahrensburg, Germany) products are foreign generators. Figures 14–17 show the experimental data obtained from a comparison with other generators. Figure 14 shows the ABB data; Figure 15, the BASLER data; and Figures 16 and 17, the designed generator's data.

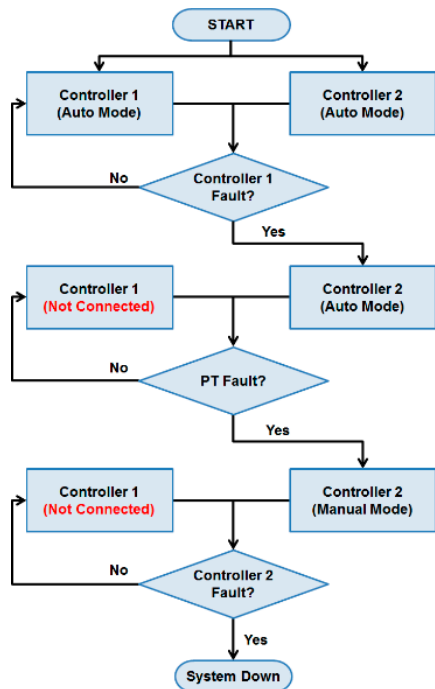


Figure 13. Diagnosis Sequence of Redundant Controller Operating Mode.

Figure 14 shows the waveform generated during the channel switchover (Company A), wherein normal voltage is restored after about 1 s.

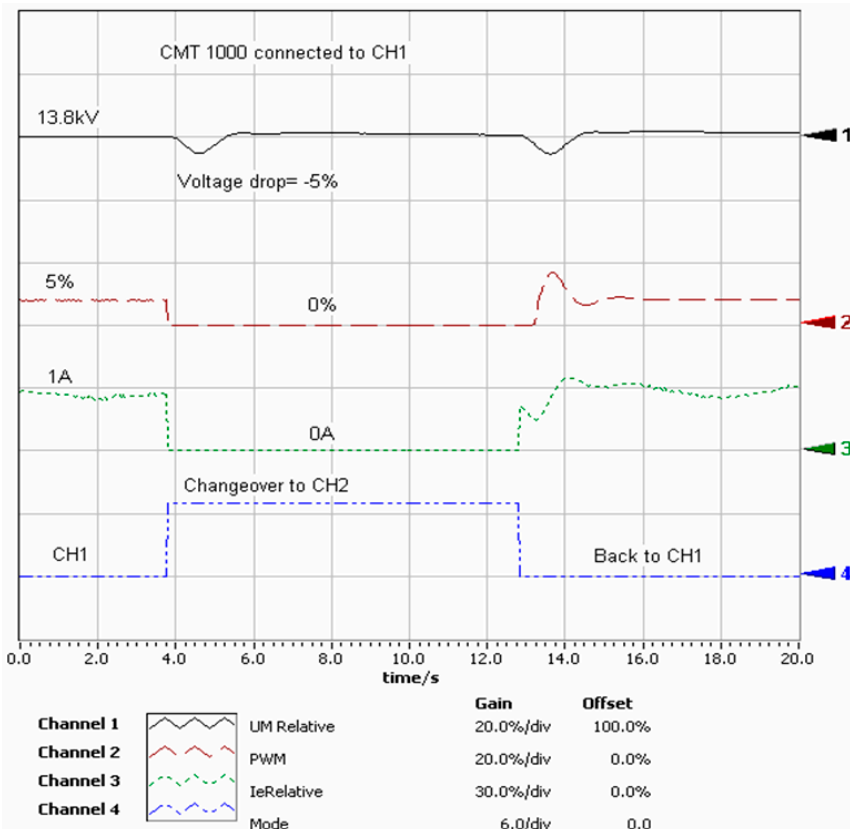


Figure 14. Controller Switchover Test (Company A).

Figure 15 shows the waveform generated during the channel switchover (Company B), wherein normal voltage is restored after about 970 ms.

Figure 16 shows the waveform generated during the channel switchover process using the algorithm [30] introduced in this study. CH1, CH2, and CH3 indicate the individual operating signals of Controllers 1, 2, and 3, respectively. The switchover time from Controller 1 to Controller 2 was 12 ms.

Analysis (Real-Time Monitor)

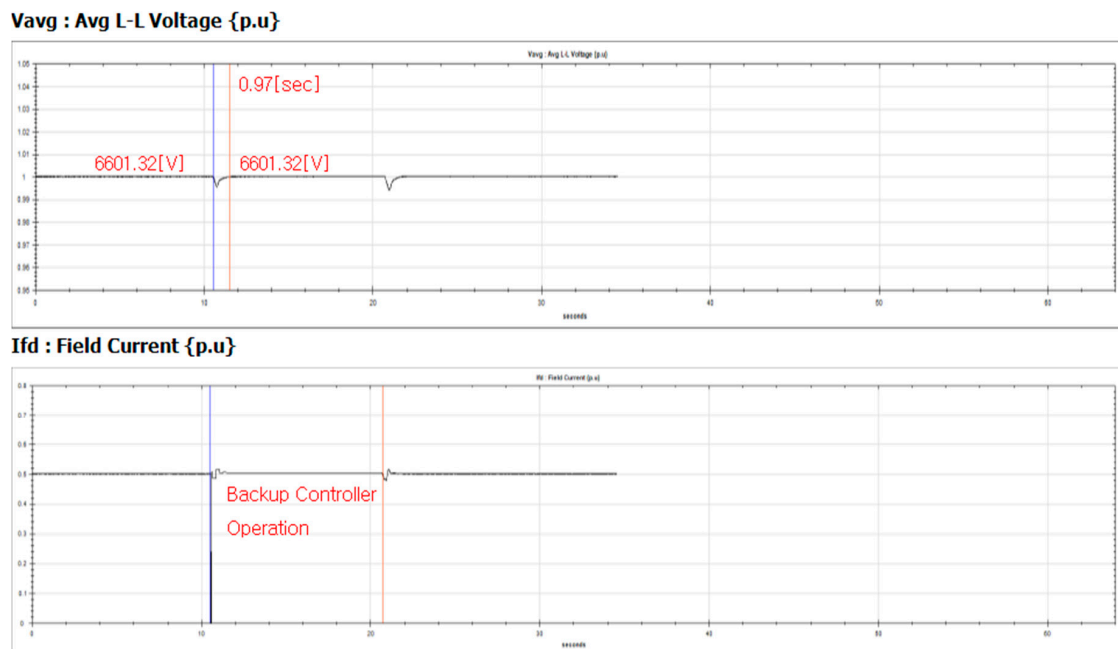
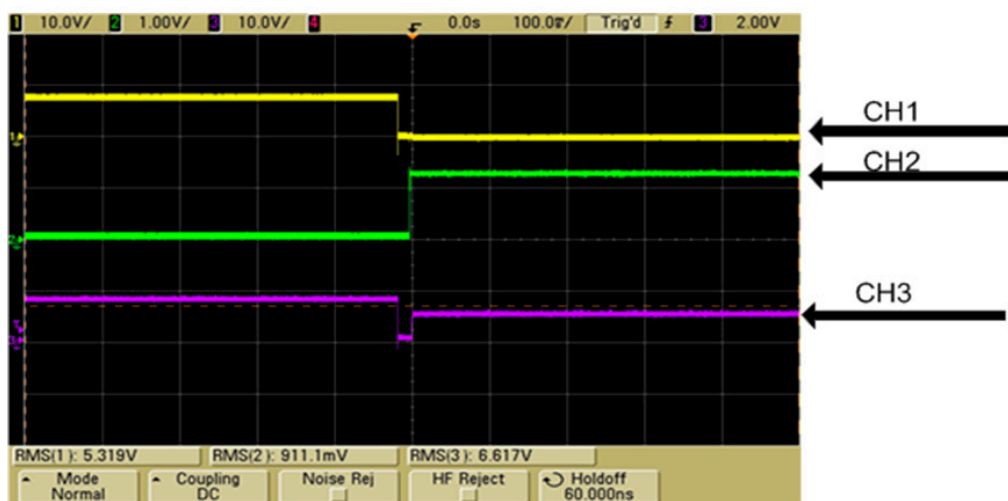


Figure 15. Controller Switchover Test (Company B).



CH1 : Controller 1
CH2 : Controller 2
CH3 : Output

Figure 16. Switchover Test of Redundant Controllers.

Figure 17 shows the waveform generated during the field test. The voltage dropped instantaneously but returned to its normal state within 16 ms.

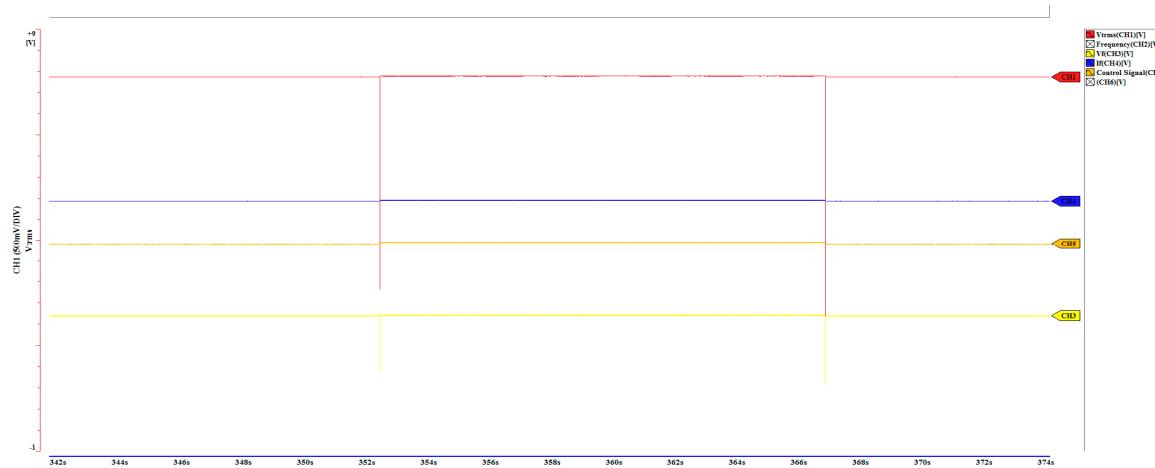


Figure 17. Redundant Controller Switchover at the Field Test.

When testing a redundant system, it will help stabilize the system more effectively if it enters the stabilizing range within one cycle. In other words, the system changes over within 16.666 ms (60 Hz * 1 cycle) so that normal control can be initiated in the next cycle.

Therefore, when testing the redundancy, a signal entering the range of stabilization within 1 cycle would contribute to the stability of the system. In other words, the system will be switched over within 16.666 ms (60 Hz * 1) so that normal control can be resumed in the next cycle.

5. ETAP Simulation

The simulation algorithms used for the digital excitation system described in this section are able to identify the operating characteristics by programming them as an ETAP program. Although a test for a small-signal disturbance can be conducted at the testing site at present, the same cannot be carried out for a fault wave. Thus, to solve this problem, the response characteristic of an excitation system is identified by using an ETAP program.

There are many power system analysis programs being used in the Republic of Korea. In a system consisting of several systems operating organically, it is necessary to check each system accurately so that, from a mechanical perspective, the library of a commercial program such as ETAP can be used to validate the excitation system for which it is often difficult to conduct a test in the actual situation. For this reason, such system analysis program was used to check the responses to the controller.

Simulations were conducted after simulating the power system of a power plant by using the proposed methodology and the power system analysis program ETAP. The simulations focused on operating situations wherein both the OEL and UEL functions were or were not used. For the simulations, $\pm 10\%$ of the normal system voltage was used.

5.1. ETAP Simulation of the Proposed System

The basic functions of a common excitation system were designed for the simulations. The simulation conditions excluded both OEL and UEL functions, and the system voltage limits were set at $\pm 10\%$.

5.2. ETAP Simulation of OEL

OEL was designed, and experiments were conducted by comparing the situations wherein the controller including the OEL was or was not used. The power voltage was reduced by -10% for 15 sec to check the operating status.

Figure 18 depicts the waveform showing the variations in the generator power phase angles. There was variation of 2.51° in the model without the OEL and variation of 0.77° in the model with the OEL.

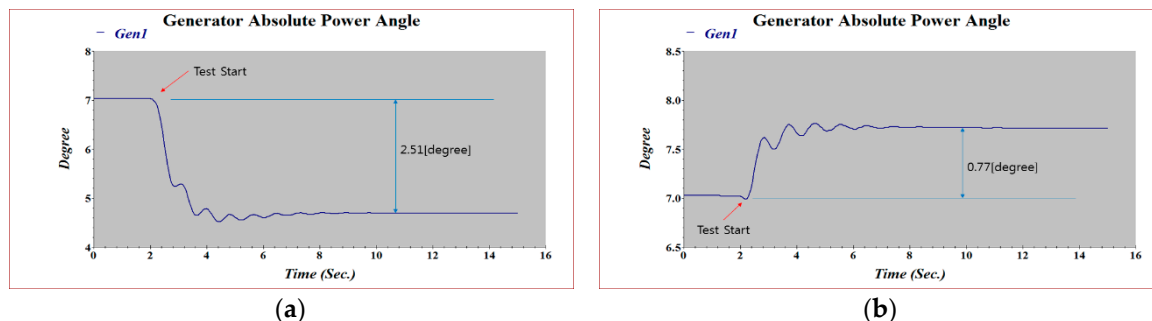


Figure 18. Generator Power Phase Angles with/without OEL. (a) Without OEL at -10% Impact in Grid; (b) With OEL at -10% Impact in Grid.

The response characteristics of the excitation system can be identified by the results of the ETAP simulations, and they can contribute to the stability of the entire power system.

The response characteristics of an excitation system can be confirmed based on the result obtained from the simulation model; with this result, it is possible to stabilize the entire power system by collaborating with the protective relay.

Figure 19 shows the generator's reactive power. Since the field current flowed more when the system voltage was constant, the reactive power (lagging) increased by as much as 7.733 Mvar. On the other hand, the model without OEL showed no increase in reactive power since its field current had been limited.

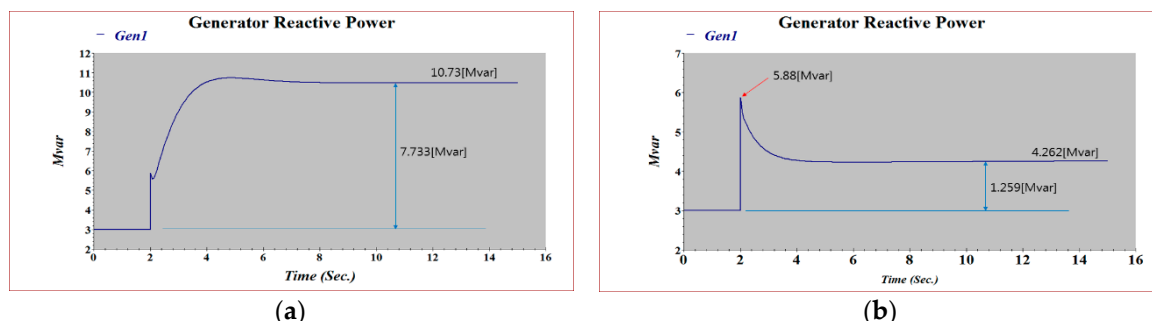


Figure 19. Generator Reactive Power with/without OEL. (a) Without OEL at -10% Impact in Grid; (b) With OEL at -10% Impact in Grid.

The waveform of the generator's active power is shown in Figure 20. Since the active power output is controlled by the governor, the waveforms of the models with or without OEL are similar.

As can be seen in the waveforms of active power shown in Figure 20, the generator speed becomes constant when governor control is constant. Figure 21 shows that the variation in the generator's RPM (Revolution Per Minute) was 0.0002% , which can be interpreted to mean that there were no changes.

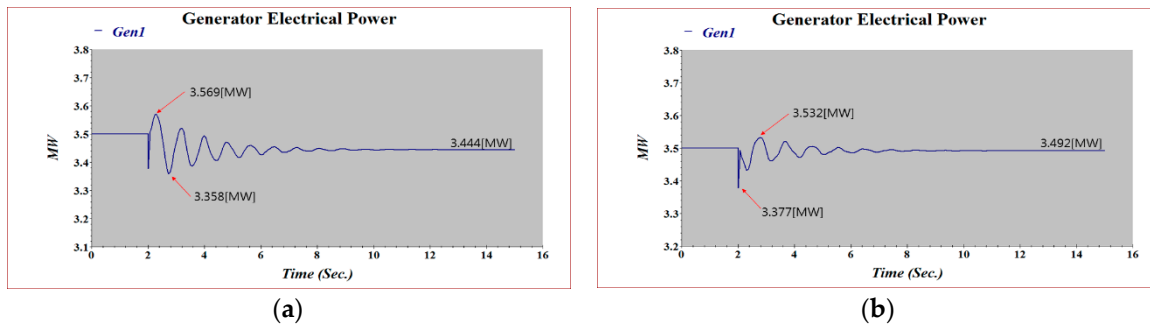


Figure 20. Generator's Active Power with/without Over Excitation Limiter (OEL). (a) Without OEL at -10% Impact in Grid; (b) With OEL at -10% Impact in Grid.

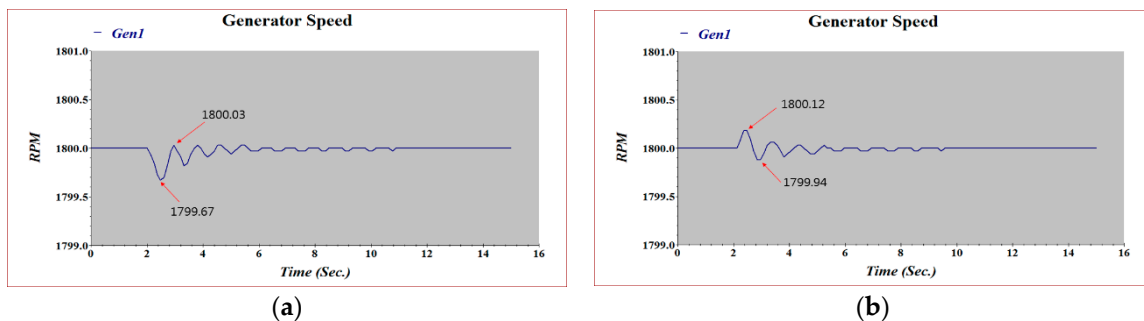


Figure 21. Generator Speed with/without OEL. (a) Without OEL at -10% Impact in Grid; (b) With OEL at -10% Impact in Grid.

The waveform in Figure 22a shows that the generator current increases by approximately 140% in compensation when the grid voltage changes by as much as -10% .

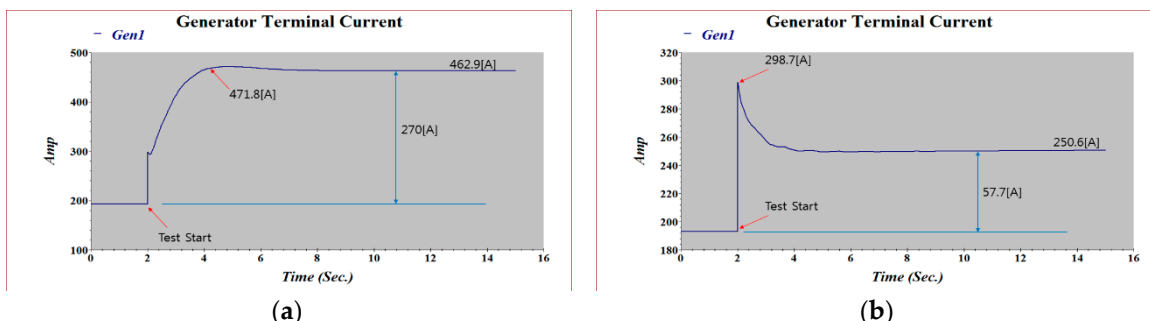


Figure 22. Generator Current with/without OEL Function. (a) Without OEL at -10% Impact in Grid; (b) With OEL at -10% Impact in Grid.

Figure 23 shows the waveform that represents the difference between voltage and frequency when the grid voltage drops by -10% . In Figure 23a, since only the generator terminal voltage was controlled, there could be an instantaneous deviation in the voltage level, but this would be restored eventually. In other words, the change in the grid voltage would be converted into the rated voltage. However, that the waveform in Figure 23b shows that the field current was controlled so that a difference of 8.1% was maintained between voltage and frequency.

The waveform of frequency shown in Figure 24 maintained the same level of speed as the generator, with minimal changes in the generator frequencies.

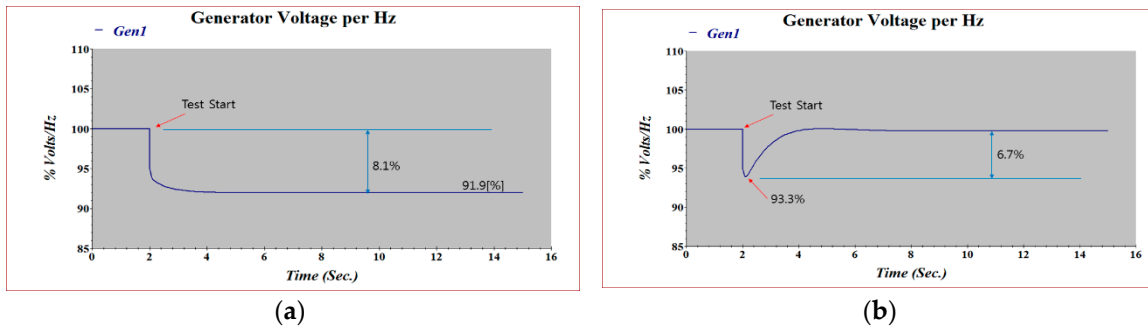


Figure 23. Generator V/Hz with/without OEL Function. (a) Without OEL at -10% Impact in Grid; (b) With OEL at -10% Impact in Grid.

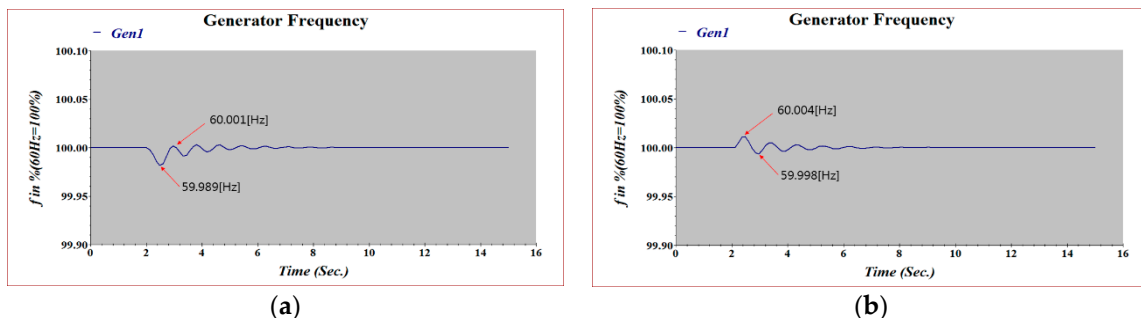


Figure 24. Generator Frequency with/without OEL Function. (a) Without OEL at -10% Impact in Grid; (b) With OEL at -10% Impact in Grid.

Figure 25 shows the waveform of generator voltage. Since the model without OEL did not limit the voltage, it instantaneously dropped from 13.8 kV to 12.963 kV but returned to the original level later. Since the model with OEL limited the field current, however, the generator voltage dropped to 12.694 kV.

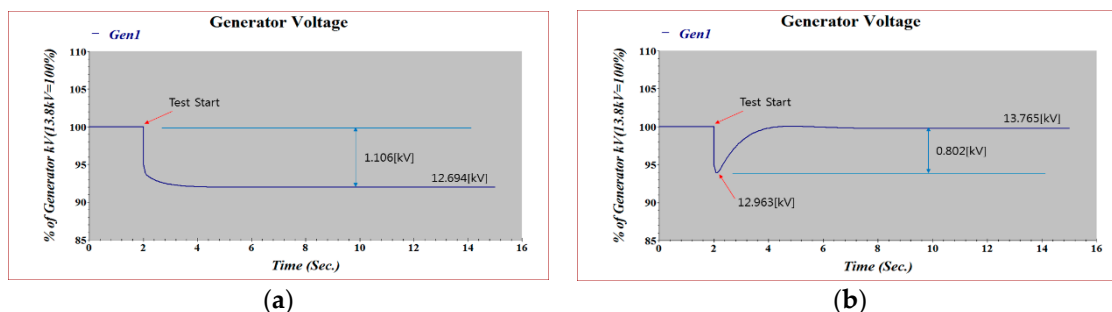


Figure 25. Generator Voltage with/without OEL. (a) Without OEL at -10% Impact in Grid; (b) With OEL at -10% Impact in Grid.

Figure 26 shows the waveform of the generator field voltage, which is quite similar to the field current waveform.

Figure 27 illustrates the primary waveform of the field current with OEL. Since the model without OEL controlled the voltage, the field current increased by about 150%. On the other hand, in the model with OEL, the field current, which instantaneously increased by about 110%, returned to its original level once the OEL kicked in.

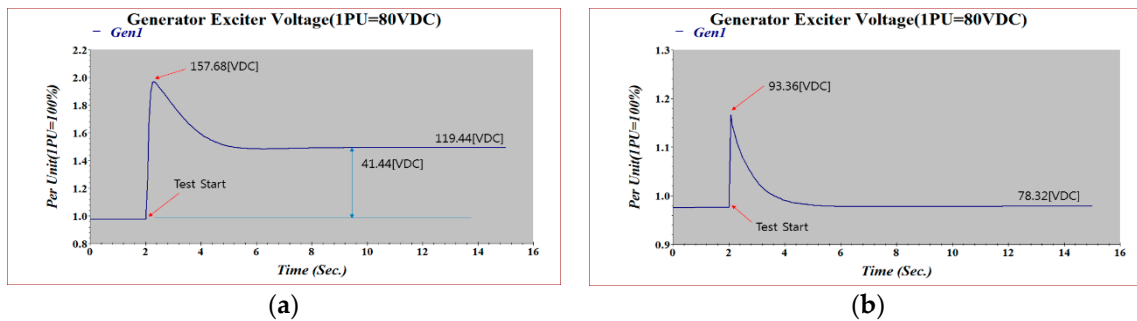


Figure 26. Generator Field Voltage with/without OEL. (a) Without OEL at -10% Impact in Grid; (b) With OEL at -10% Impact in Grid.

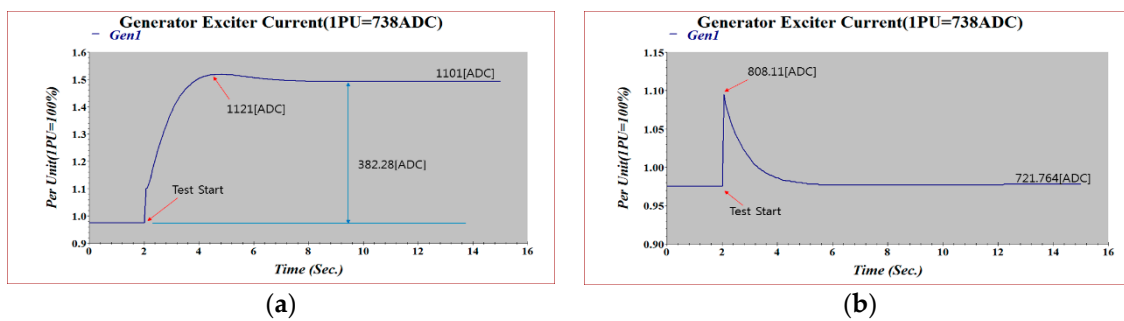


Figure 27. Generator Field Current with/without OEL. (a) Without OEL at -10% Impact in Grid; (b) With OEL at -10% Impact in Grid.

5.3. Simulation of UEL

UEL was designed, and experiments were conducted by comparing the situations wherein the controller including the UEL was or was not used. The power voltage was increased by 10% for 15 s to check the operating status.

Figure 28 depicts the waveform showing variations in the generator power phase angles. There was variation of 3.75° in the model without the UEL and variation of 2.12° in the model with the UEL.

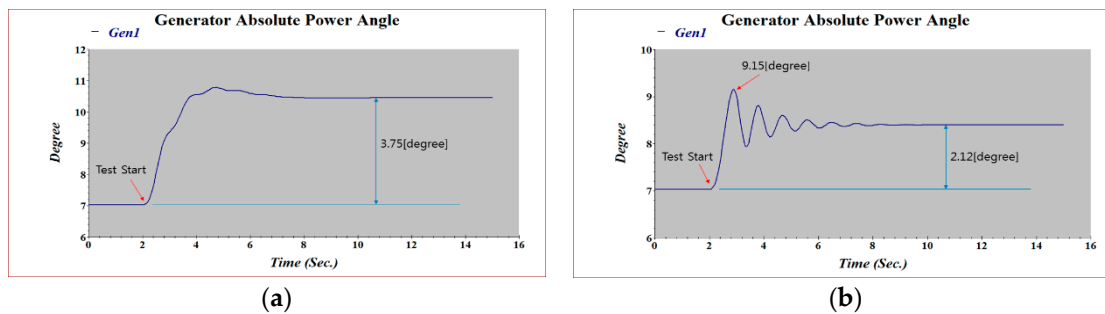


Figure 28. Generator Power Phase Angles with/without Under Excitation Limiter (UEL). (a) Without UEL at -10% Impact in Grid; (b) With UEL at -10% Impact in Grid.

As can be seen in the waveforms of active power shown in Figure 28, the generator speed becomes constant when governor control is constant. Figure 29 shows that the variation in the generator RPM was 0.0002% , which can be taken to mean that there were no changes. Figure 29 shows the generator's reactive power. Since the field current flows less when the system voltage is constant, the reactive power (leading) decreased by as much as -4.509 Mvar. On the other hand, the model with the UEL showed no increase in reactive power since its reactive power had been limited.

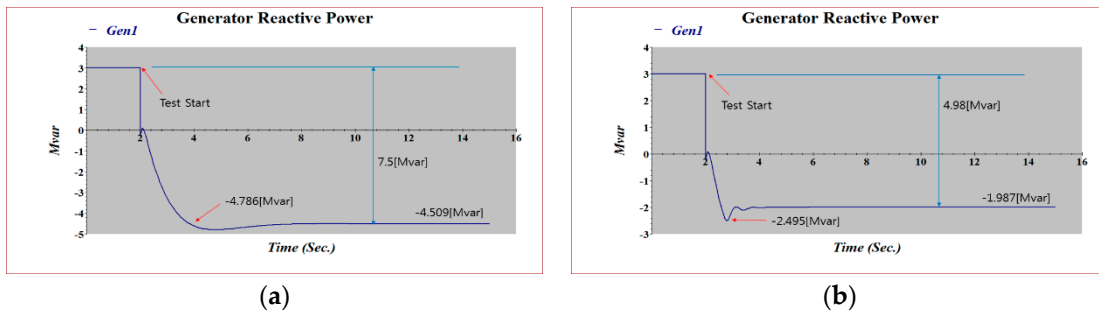


Figure 29. Generator Reactive Power with/without UEL. (a) Without UEL at -10% Impact in Grid; (b) With UEL at -10% Impact in Grid.

The main function of the UEL is to prevent the excitation system from becoming under-excited, which will cause the generator to lose its synchronism. Specifically, the UEL prevents the excitation system from becoming under-excited and dropping to a level below the set limit.

The waveform of the generator's active power is shown in Figure 30. As with the OEL, since the active power output is controlled by the governor, the waveforms of the models with or without the UEL are similar.

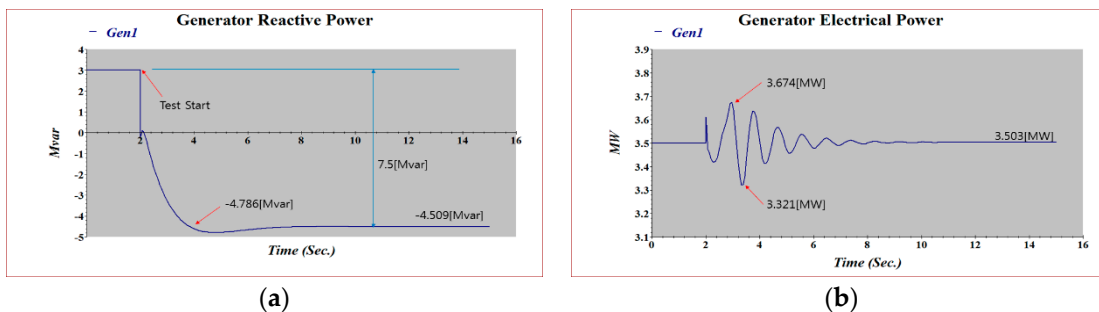


Figure 30. Generator Active Power with/without UEL. (a) Without UEL at -10% Impact in Grid; (b) With UEL at -10% Impact in Grid.

As can be seen in the waveforms of active power in Figure 30, the generator speed becomes constant when governor control is constant. Figure 31 shows that there were no changes in the generator's RPM.

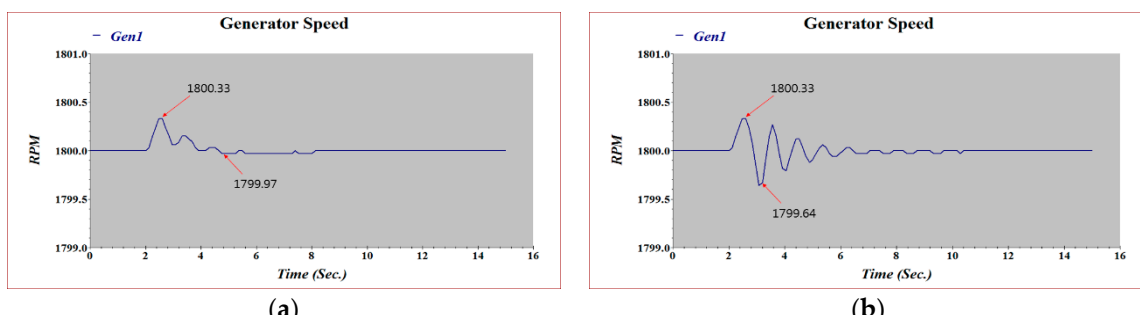


Figure 31. Generator Speed with/without UEL. (a) Without UEL at -10% Impact in Grid; (b) With UEL at -10% Impact in Grid.

The waveform in Figure 32 shows that the generator current increases for a while when the grid voltage changes by as much as $+10\%$, and then increases again.

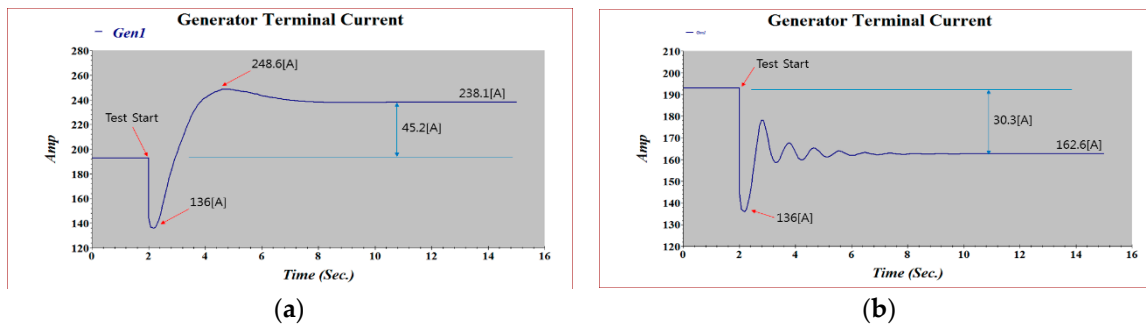


Figure 32. Generator Current with/without UEL. (a) Without UEL at -10% Impact in Grid; (b) With UEL at -10% Impact in Grid.

Figure 33 shows the waveform that represents the difference between voltage and frequency when the grid voltage is increased by $+10\%$. In Figure 33a, since only the generator terminal voltage was controlled, an instantaneous deviation in the voltage level could occur, but it would be restored eventually. In other words, the change in the grid voltage would be converted into the rated voltage. However, that the waveform in Figure 33b shows that the field reactive power was controlled so that a difference of 3.661% was maintained between voltage and frequency.

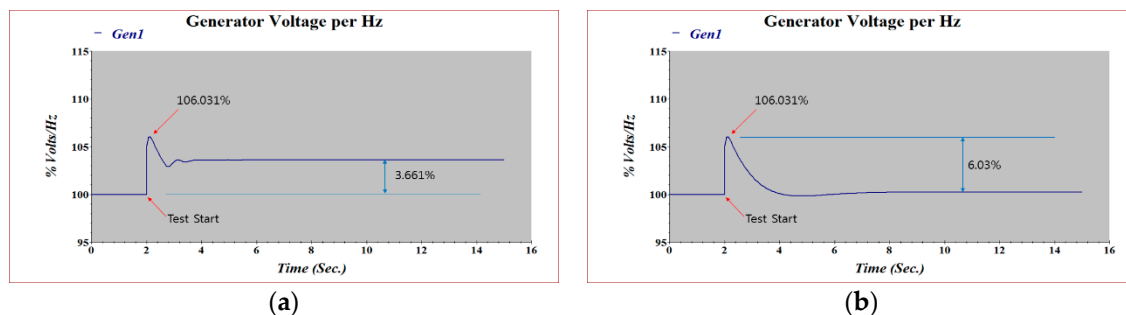


Figure 33. Generator V/Hz with/without UEL. (a) Without UEL at -10% Impact in Grid; (b) With UEL at -10% Impact in Grid.

As shown in Figure 34, the waveform of frequency exhibits minimal changes as the generator speed.

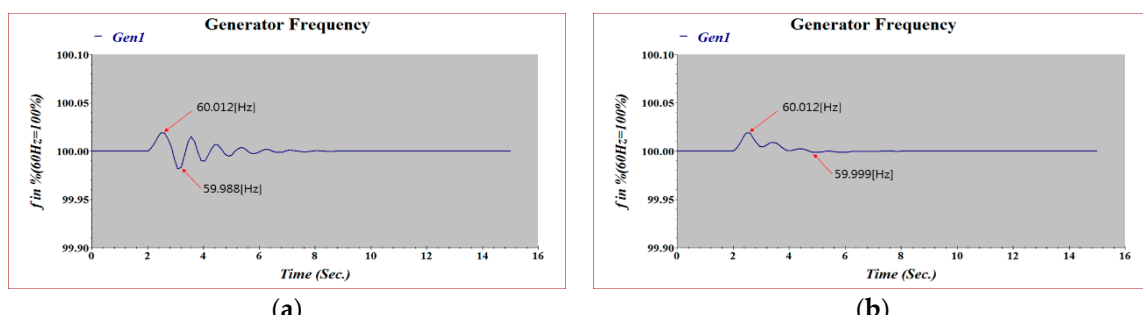


Figure 34. Generator Frequency with/without UEL. (a) Without UEL at -10% Impact in Grid; (b) With UEL at -10% Impact in Grid.

Figure 35 shows the waveform of the generator's voltage. Since the model without the UEL controlled the voltage, it instantaneously increased from 13.8 kV to 14.632 kV but returned to its original level later. Since the model with the UEL limited the reactive power, however, the generator voltage increased to 14.298 kV .

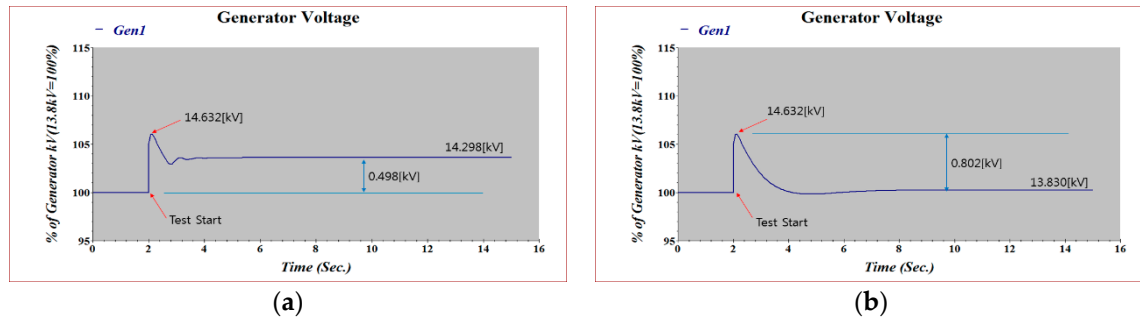


Figure 35. Generator Voltage with/without UEL. (a) Without UEL at -10% Impact in Grid; (b) With UEL at -10% Impact in Grid.

Figure 36 shows the waveform of the generator field voltage, which is quite similar to the field current waveform.

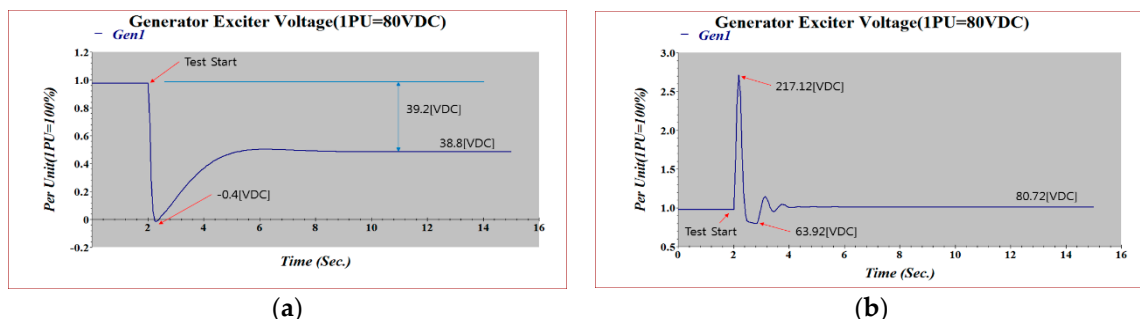


Figure 36. Generator Field Voltage with/without UEL. (a) Without UEL at -10% Impact in Grid; (b) With UEL at -10% Impact in Grid.

Figure 37 shows the primary waveform of the field current with the UEL. Since the model without the UEL controlled the voltage, the field current decreased by approximately 45%. On the other hand, in the model with the UEL, the field current, which instantaneously decreased or increased, became constant once the UEL kicked in.

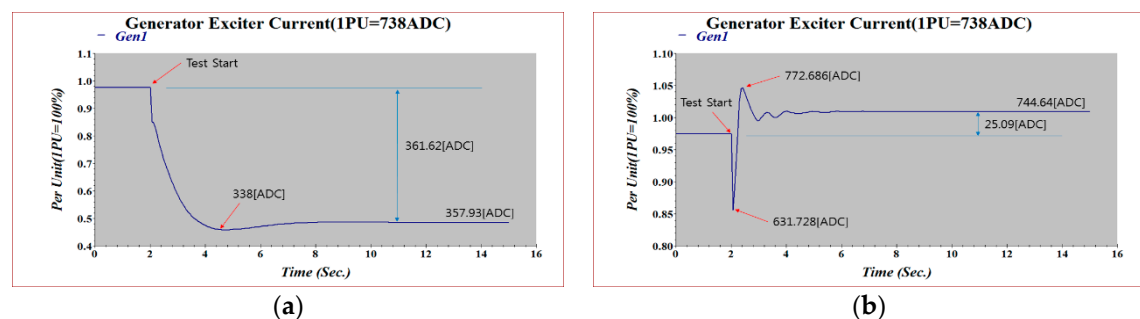


Figure 37. Generator Field Current with/without UEL. (a) Without UEL at -10% Impact in Grid; (b) With UEL at -10% Impact in Grid.

5.4. Field Test and Results (37 kW DC Motor Start Control)

In the event of a power system failure, emergency power is supplied from the battery panel(s) to start the DC motor so as to supply power to the major facilities. This was tested with field test and simulations wherein a PSIM program was used.

5.4.1. Principle of DC Motor

The “DC Motor Start” function allows the DC motor to start quickly in case of emergencies at the power plant to supply power in order to protect the generating units.

Compound DC motors can be controlled separately since their armatures and magnetics are separated. Their operating characteristics can be expressed by the following equations:

$$\Phi = \int (I_f), \quad (1)$$

$$T = k \times \emptyset \times I_A, \quad (2)$$

$$U_d = E + R_i \times I_A, \quad (3)$$

$$E = k \times n \times \emptyset, \quad (4)$$

$$n = k \times E = (U_d - R_i \times I_A) / (k \times \emptyset), \quad (5)$$

Φ : Magnetic flux of motor

I_f : Field current

T : Axial torque of motor

k : Proportional constant

I_A : Armature current

U_d : Armature voltage supplied

R_i : Armature circuit resistance

E : Motor BEMF

n : Rotation velocity.

Ordinarily, a constant magnetic flux should be maintained for motors, and this can be achieved by maintaining a constant field current. Equation (2) shows that, when the motor output torque is greater than the load torque, the extra torque becomes an acceleration torque and pushes the speed of the motor. At the same time, the output torque increases when the armature current increases. Thus, Equation (3) shows that the armature current changes according to the armature voltage supplied; Equation (4) suggests that the motor BEMF (Back ElectroMotive Force) is proportional to the speed, and Equation (5) illustrates that the motor speed is proportional to the armature voltage supplied and the motor magnetic flux is inversely proportional to the field current.

The rated speed at the maximum level of magnetic flux and BEMF is called the base speed, but it can be increased further if the field current is reduced. This is called Field Weakening, and the motor runs in this domain.

The AVR (Auto Voltage Regulator) and the UEL (Under Excitation Limiter) are automatically controlled at 180 Hz, whereas the FCR (Field Current Regulator) and the OEL (Over Excitation Limiter) are manually controlled at 360 Hz, respectively. The control system has been designed in such a way that the control signals are transmitted within the 6-pulse cycle ($60 \text{ Hz} \times 6 = 360 \text{ Hz}$) of the phase-controlled rectifier. This was necessary to check the integrity of the controller by confirming that the control loop is operating normally.

Figure 38 shows a schematized form of the OEL model. The overexcitation protector is a controller consisting of a proportional integrator operating as an overcurrent limiter designed to be operated for the online or offline V/Hz limiter first. The overcurrent limiter operates by selecting an adequate value among the setpoints depending on the situation to maintain a value lower than a certain value against the field current. The setpoints include offline overcurrent limit values, online primary overcurrent limits, and online secondary overcurrent limits. The control objective of the overexcitation limiter in the off-line situation where the generator has been paralleled off is to prevent the occurrence of an excess magnetic flux in the generator and each transformer connected to the generator. On the other hand, in the online situation where the generator has been paralleled in, the objective is to prevent any damage to the field winding due to overheating.

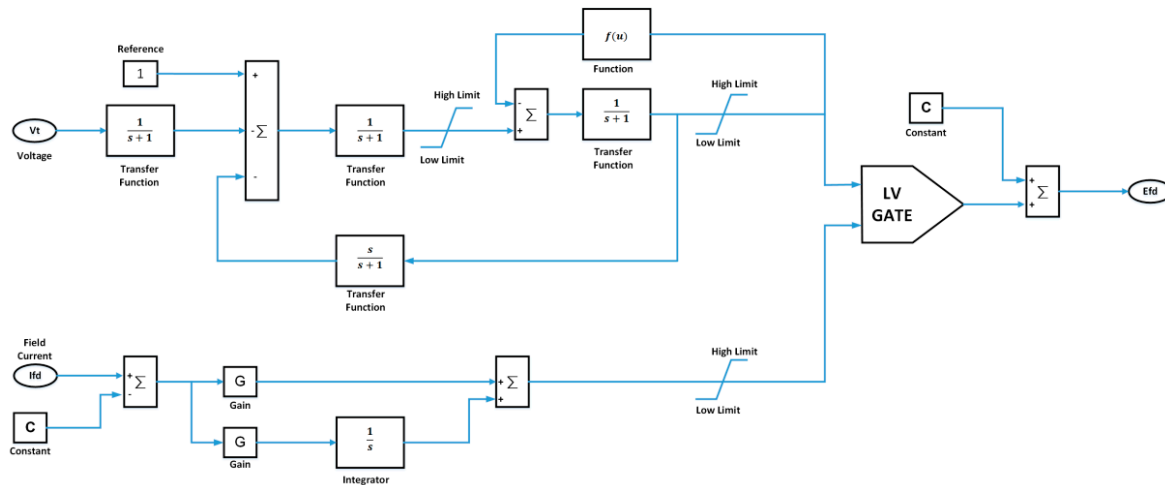


Figure 38. Schematized Form of the OEL Model.

Concerning the operating process of the overexcitation limiter, when the output is lower than that of the manual voltage regulator or the automatic voltage regulator, an alert will be fired in HMI, and the firing angle of PCR (Phase Controlled Rectifier) will be decided by the output of the overexcitation limiter. In this situation, the process will continue until the output of the automatic (manual) voltage regulator becomes lower than that of the overexcitation limiter by lowering the setpoints of these regulators. In other words, the main function of the OEL model is to prevent overheating beyond the cooling range of generator field magnetics due to excessive current flow, having a setting function based on the field current/time function.

Figure 39 shows a schematized form of the UEL model. When a leading-phase operation is performed by lowering the voltage of the synchronized generator (i.e., operating in the under-excitation area on the generator capacity curve), it will lead to overheating in the generator armature core as well as a drop in the generator static stability. The former is caused by the following phenomenon: a leakage flux at the end of the generator stator winding enters vertically against the stator core lamination such that an eddy current can be generated at the core end, which will then be partially overheated. In a state of overexcitation operation (lagging power factor), the operation will be performed in a condition wherein the retaining ring at the field magnet end is saturated so that there will not be much of a problem since the scale of the leakage flux is not that large. In under-excitation condition (leading power factor), however, the retaining ring will not be saturated since the scale of the field current is small, so the magnetic flux at the end of the stator winding enters following the axial direction of the armature core; thus causing larger leakage. Additionally, in this condition, since the magnetic flux generated by the stator winding current merges with the magnetic flux generated by the field current, partial overheating at the stator end can be a problem, especially becoming the main cause of largely limiting the operation range of the generator using a cylinder-type field magnet. A static stability limit indicates the maximum active power that can be supplied to the system at steady field voltage.

It is actually possible to increase these limits considerably with a rapid automatic voltage regulator, but the operating point of the generator should always be kept within a safe range to prepare for the switchover from automatic to manual operation since the responsiveness of the manual voltage regulator is often designed to be slower than that of the automatic voltage regulator. Between the two aforesaid problems occurring while operating in under-excitation condition (i.e., leading phase operation), the restriction due to mechanical heating can be considered a more serious issue than securing static stability. The generator capacity curve is often referred to when considering the functions of the UEL. To prevent overheating at the end of an armature core, the operating point should be set by leaving a margin of 5~15% from the limit line of the phase-leading area. In other

words, the main function of the UEL model is to prevent partial overheating at the stator core due to the concentration of magnetic flux within the generator caused by the armature reaction while operating in the phase-leading area.

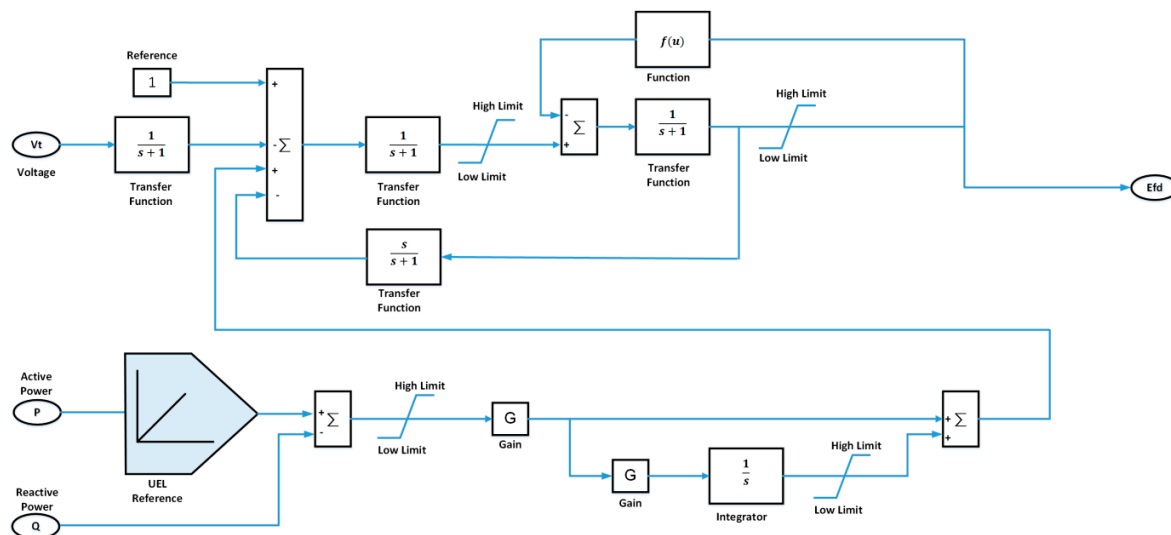


Figure 39. Schematized Form of the UEL Model.

5.4.2. Specifications of DC Motor

Table 1 shows the specifications of the DC motor's startup panel. The 3-phase rectifier maintains the voltage at DC 240 V by receiving 3-phase AC voltage. The automatic startup resistor panel consists of a number of resistors (MC1–MC6) and a controller that allows the rated field current to flow. Initially, the starting rheostat (R_A) supplies power to the DC motor panel with a 1 s delay after receiving a "Start" signal via the MC1 main power supply contactor. The startup current is limited from MC2 to MC6, starting the motor after all the processes have been completed sequentially (On state). Moreover, if there is any armature resistance (R_a), the data of the motor will show a value of 0.0153Ω .

Table 1. Specifications of the DC Motor.

kW	37	VOLT	240
ARM AMPS	170	FIELD AMPS	1.87
FIELD VOLT	240	FIELD OHMS 25 °C	90
RPM	1780	TYPE	CDL409AT

5.4.3. Startup Current Limit

A startup rheostat (R_A) should be selected to satisfy the 200% startup current limit, setting it at 0.7Ω and 10 kW. The startup resistance can be calculated as shown below. Since the motor speed at the time of initial startup is "0," the armature BEMF is also "0". Thus, the resistance can be estimated by the following equation:

$$240Vdc = (R_A + R_a) \times (170A \times 200\%), \quad (6)$$

The armature resistance is 0.0153Ω (motor data), so the startup resistance (R_A) can be calculated as follows:

$$R_A = \frac{240V_{dc}}{170A \times 200\%} - 0.0153 = 0.7058 - 0.0153 = 0.69 \Omega, \quad (7)$$

∴ Considering the tolerance, R_A is set at 0.7Ω . Since the startup current becomes 170 amp after gradually decreasing from 350 amp over a period of 30 s, the capacity of the resistance can be calculated by assuming that an average of 260 amp flows for a period of 30 s.

$$Watt_{R_A} = I^2 \times R_A = 260^2 \times 0.7 = 47.32 \text{ kW}, \quad (8)$$

However, that the value obtained from Equation (8) does not consider the duty rate. Moreover, since a little less than one minute of resistance is required, $1/5$ of this value (approx. 10 kW) is sufficient to satisfy the startup condition.

5.4.4. Simulation and Field Test

As shown in Figure 40, a PSIM simulation circuit for the DC motor startup control was created. In ①, DC240V is entered as the power supply for the DC motor startup; in ②, data related to the DC Motor are entered. Finally, ③ corresponds to the startup resistance panel for the DC Motor startup control.

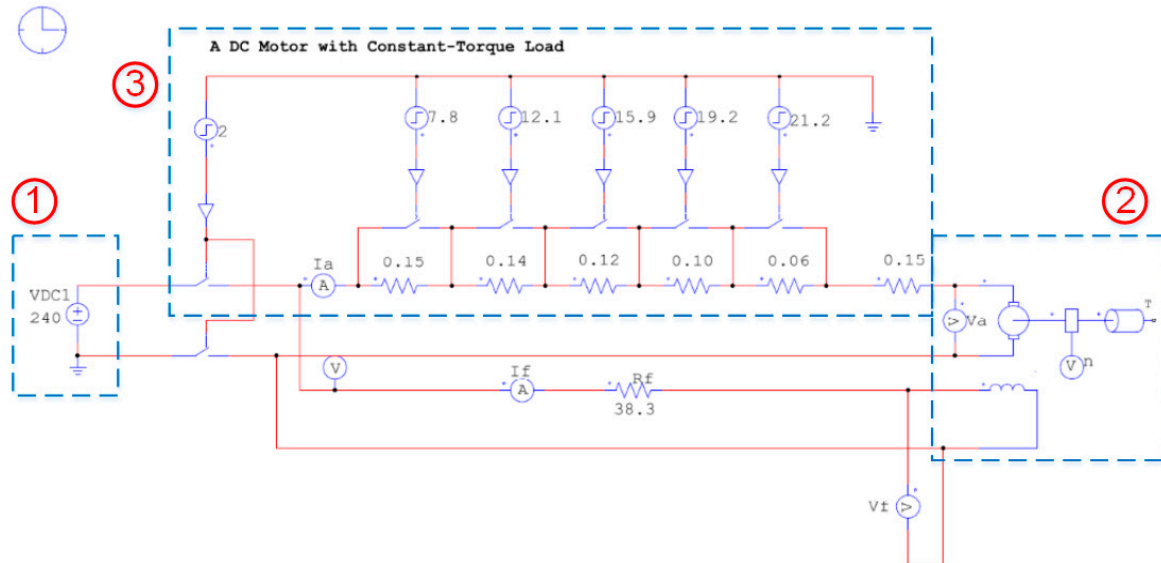


Figure 40. PSIM (Powersim inc.) Simulation Circuit for the DC (Direct Current) Motor.

Figure 41 is a block diagram of the excitation system of synchronous motor architecture. The motor consists of the main motor, motor circuit breaker, breaker panel with a 42-reactor bypass, reactor that limits the startup current, excitation transformer that supplies power to the excitation system, and controller that controls the field current of the motor. The synchronous motor is run by the torque generated by the interaction between the magnetic field of an air gap created at the pole by the direct current and the alternating current of an armature. Since the latter changes its direction every half-cycle, the pole also rotates in the same way so as to be in synch with the alternating current. This way, it gains rotational force (torque) by continuously moving in the same direction.

Figure 42 shows the operation time chart of an existing excitation system. When the operator presses the start button, the 52S-motor circuit breaker of the synchronous motor will be activated; once deployed, the reactor starts first, followed by a decline in current due to the acceleration exceeding the constant speed. At this time, the 42-breaker installed parallel with the reactor is deployed to operate

the motor continuously. In the existing excitation system, the field current is supplied with some startup delay (t -sec) using the timer-relay mechanism. Figure 42 shows the measured waveform of the induced voltage of the excitation system rotor when startup is being carried out. It was possible to confirm that the induced voltage was 1.030 Vac, which is about 5 times greater than the rated field voltage. At this time, the tap of the reactor was set at 65% so that the voltage would not exceed 1334 Vac. The tap can be set at 50%, 65%, or 70%. When the rotor reaches the synchronous speed, the induced voltage on the rotor will become “0” as observed in the waveform shown in Figure 42. This point becomes the reference point for the pull-in current in the excitation system. In other words, the field current will be flown in to start the motor after confirming that the induced voltage has become “0”. However, that timer-based methods often fail to start the motor due to untimely activation of the field breaker or inactivation caused by timer failure or malfunction.

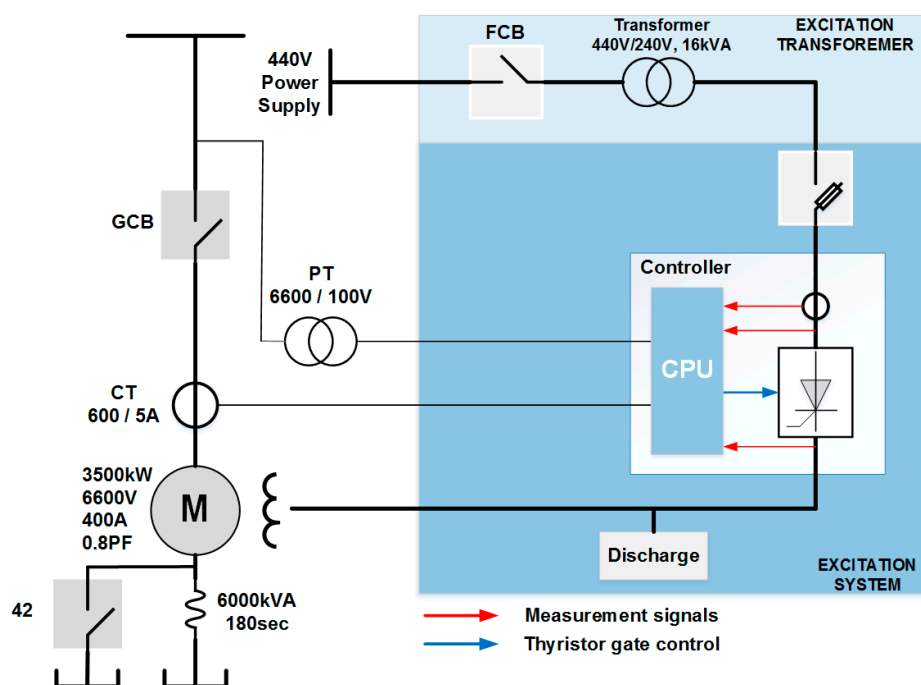


Figure 41. Composition of the Excitation System of Synchronous Motor Architecture.

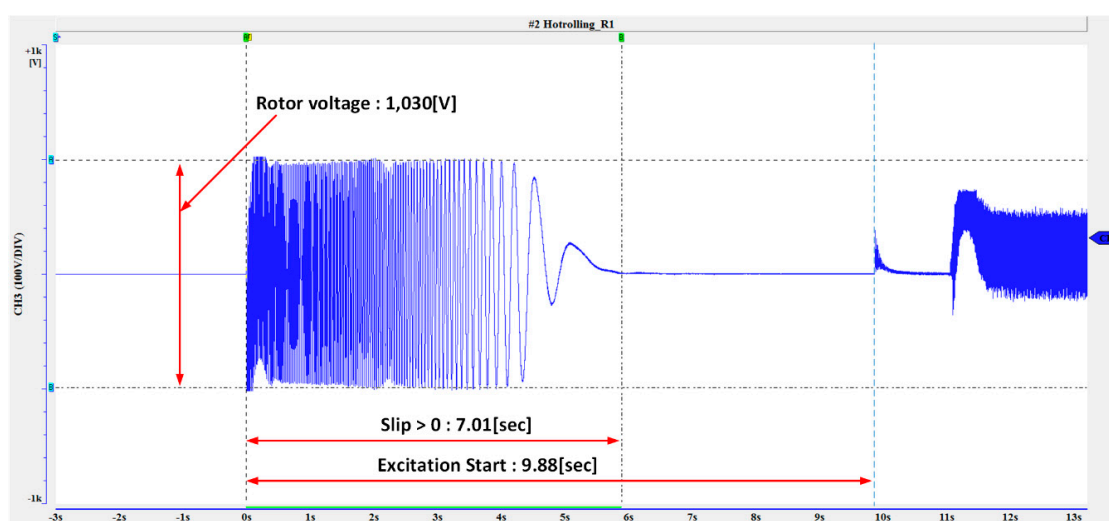


Figure 42. Startup-checking Waveform of the Existing Excitation System.

Proposed Excitation System

Figure 43 shows the operation time chart of the proposed excitation system, which guarantees stable startup characteristics by starting the motor through the measurement of the rotor slip. The proposed system is a digital excitation system that offers a high level of startup reliability; its internal startup sequence is shown in Figure 44.

At the preparation stage, the current status of the excitation system and the external protection relay is indicated; when they are in a normal state, an external digital signal ‘Release Motor Start’ will be entered. Otherwise, if ‘AUX Ready’ is ‘No’, the excitation system stops the startup process. In a normal operation process, the system startup command is entered externally; after receiving this signal, a field breaker activation command will be given. Once the breaker deployment command signal feedback has been confirmed, the starting resistor will be activated. At this time, the signal is transmitted until a Firing Signal is outputted. A 52-motor circuit breaker is then deployed after confirming this signal externally. After receiving this circuit breaker signal, the difference in frequencies of the voltage supplied from the excitation transformer and the induced voltage of the field will be measured. If the final slip value obtained from all these processes remains within the range of 2%, the rotor converges with the synchronous speed. In other words, this point is regarded as the current pull-in reference point of the excitation system, so the firing signal will be transmitted. Figure 42 shows the startup sequence of the synchronous motor.

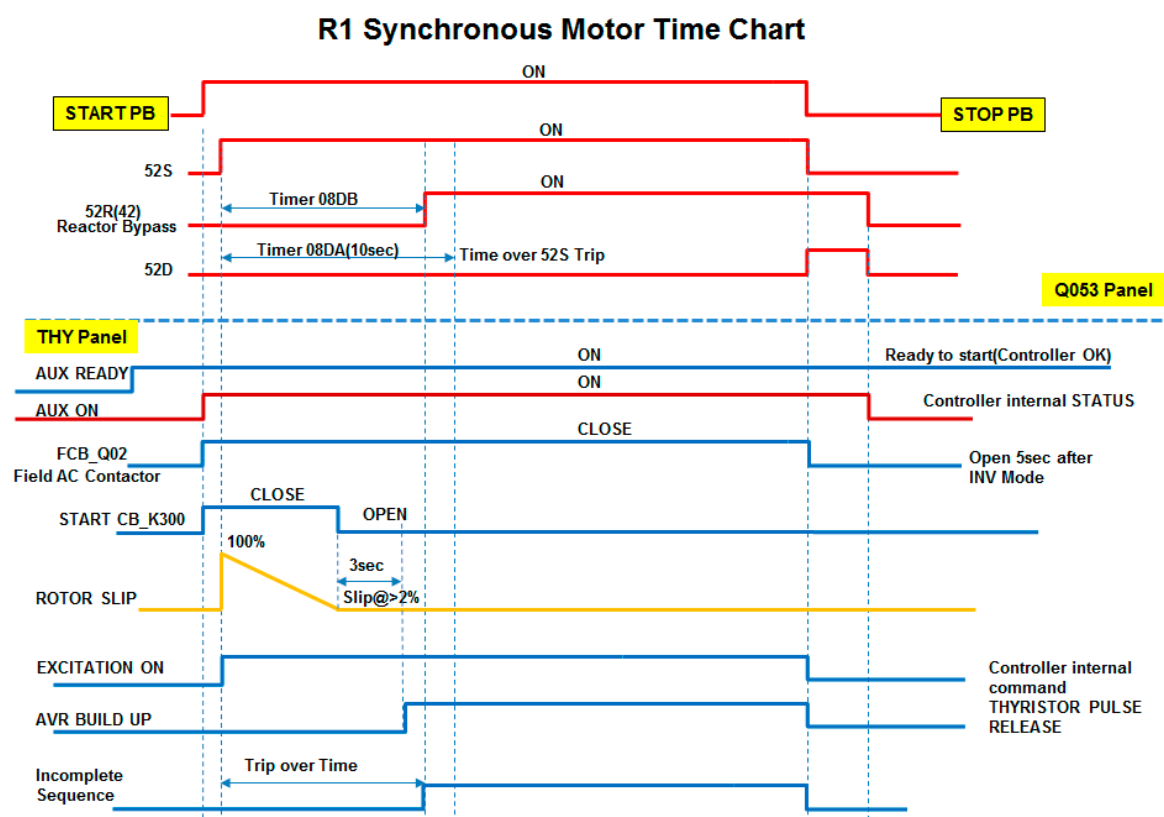


Figure 43. Time Chart of the Proposed Excitation System.

The equipment run by a system that adjusts the DC current of a field coil to control the output voltage of a generator is important due to its effectiveness in improving the quality of electricity and stabilizing the power system. The equipment relies on its technical stabilization and reliability, significantly affects the users of electricity including industry and the public, and requires advanced techniques related to the power system. After discussions about the problems that occur during the

operation of the digital excitation system as well as all types of generators, equipment protection and accident prevention have been made possible.

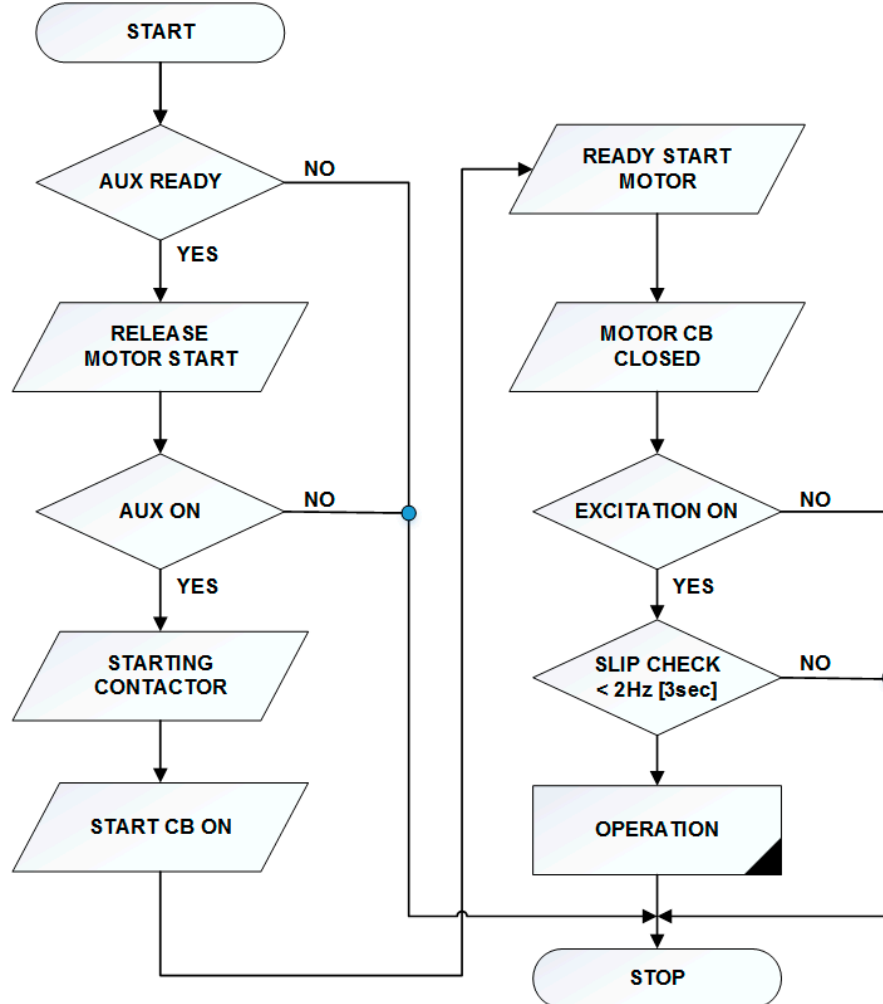


Figure 44. Startup Sequence of the Synchronous Motor.

The generator proposed in this paper has the Watch Dog Timer function, the heart of the generator. If the Watch Dog Timer does not receive periodic pulse signals within a set time, it determines that the generator in the excitation system is not functioning properly. In that case, the abnormal operation of the digital controller or the operator results in the arbitrary sending of switchover signals to switch the generator to the master/backup controller. The backup controller adopts the RS-422 communication method to follow the signals of the master controller, and if problems occur in one of the controllers, i.e., DSP or FPGA, the Watch Dog Timer detects them.

In Figure 45, a circuit was created to measure the excitation system slip. After receiving the alternating voltage induced in the field for rectification, it was converted from 0 to 10 VDC input voltage that can be received with the controller. Meanwhile, the slip is defined by the difference between the synchronous speed and the operating speed, which can be expressed as a percentage of rotation or synchronous speed in the same frequency, as shown below.

$$s = \frac{n_s - n_r}{n_s}, \quad (9)$$

n_s : Stator Electricity (Magnetic Field) Speed n_r : Rotor (Rotation) Machine Speed.

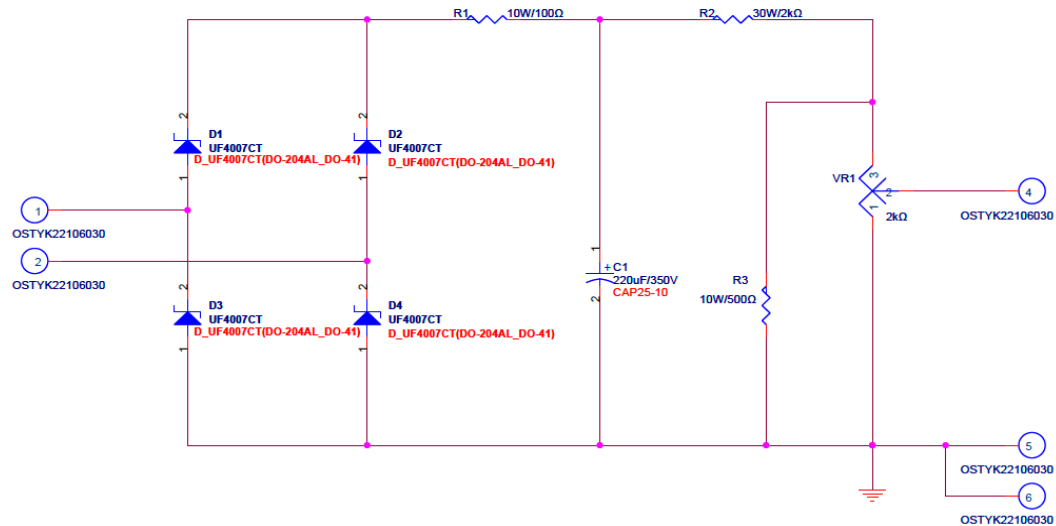


Figure 45. Circuit for Slip Measuring.

Field Test

A field test was conducted to verify the proposed excitation system using a synchronous motor of company P in ROK. Table 2 shows the motor's specifications.

Table 2. Specifications of the Synchronous Motor (Synchronous Motor).

Parameter	Value
Output	3500 (kW)
Rated Voltage and Frequency	6600 (V), 60 (Hz)
Field Voltage and Current	220 (V), 305 (A)
Power Factor	0.8

Figure 46 depicts the wave pattern of the motor's excitation system. By measuring the field voltage slip, the field current was confirmed to have increased after entering a motor start signal. While the existing system took 9.88 s to start the motor due to the characteristics of the timer used, the slip-measuring method took only 4.88 sec; thus shortening the start time. Notably, such method can guarantee stable startup by initially preventing the DC field current from being supplied at a faster rate than the synchronous speed.

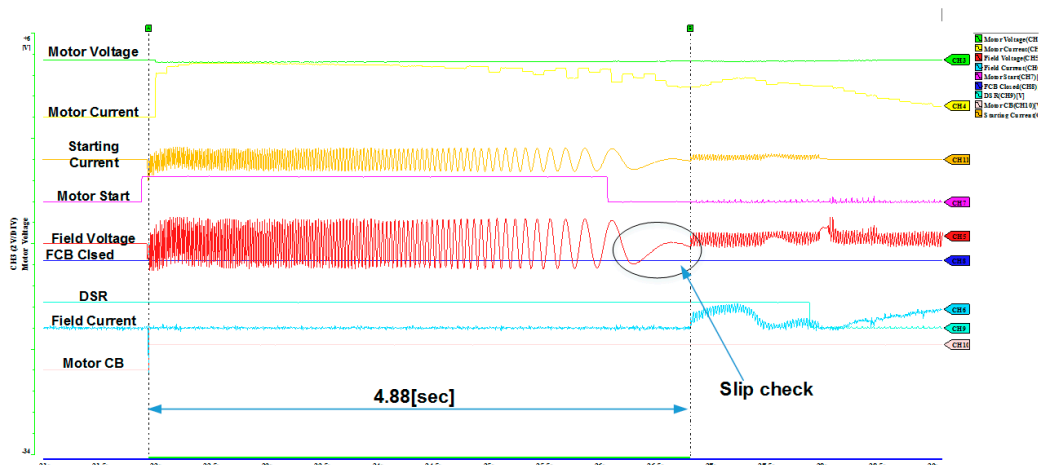


Figure 46. Synchronous Motor Startup Waveform.

6. Performance Evaluation

In this section, the operating characteristics can be identified by conducting a field test for a small signal as long as it does not damage the generator. The test for a fault wave was conducted using the ETAP program instead of performing it at the site.

The experiment on the domestic excitation system used an actual site generator or a simulator. An excitation system manufactured in Korea was applied onsite after product verification by a simulator. The excitation system experiment with a generator entailed certain risks and consumes an expensive amount of fuel, and many losses were incurred due to damage to the devices. Therefore, as the generator test simulator and EATP program are generally used to verify current domestic excitation systems, they were used to verify the proposed system.

The site tests of the simulation model and the excitation system proposed in this study were successful at some of the nuclear, thermal, and hydroelectric power stations as well as industrial sites. The Test Bed experiments using the system included its application to the gas turbine generator at the Bundang Combined GT#1 Thermoelectric Power Station and the synchronous motor in one of the industrial sites. The trial run at the former site proved that the test bed experiment using the proposed simulation model could also be successful.

Below is a test of stopping the generator normally with the controller at the actual power station. An overvoltage tripping function was embedded to prevent the excessive generation of voltage.

6.1. Controller Protection Test

The test condition for the OVT (Over Voltage Trip) test sought to check whether tripping occurs in “GCB Open” state, which was created by impressing 1.2-fold of the rated voltage at the rated frequency of 60 Hz with a KDR-1200D input PT signal. The result is shown in Table 3, where flexible performance within 2 sec was confirmed.

Table 3. Over Voltage Trip Test.

Test	Input	Time/Result	Judgment
Over Voltage Trip Test	Measuring by impressing a generator voltage trip set value of 1.2 PU	Vt: 1.2 Pu, 60 Hz Within 2 s/Confirmed	Pass

The test condition for the V/Hz test was to check whether tripping occurs when changing the frequency at the rated voltage with a KDR-1200D input PT signal. The result is shown in Table 4, where flexible performance within 5 s was confirmed.

Table 4. V/Hz TRIP Test.

Test	Input	Time/Result	Judgment
V/Hz TRIP Test	Measuring by changing the frequency at the rated generator voltage	Vt: 1.0 PU, 45 Hz TRIP Approx. 5 s/Confirmed	Pass

The test condition for the V/Hz test sought to check whether tripping occurs when changing the KDR-1200 input field current in “GCB Open” state. The result is shown in Table 5, where flexible performance within 2 s was confirmed.

Table 5. OET Trip Test.

Test	Input	Time/Result	Judgment
OET Trip Test	Measuring by adjusting the generator field current	IF: 0.4000 U TRIP Approx. 2 s/Confirmed	Pass

The test condition for the V/Hz test was to check whether tripping occurs when changing the KDR-1200 input field current in “GCB Close” state. The result is shown in Table 6, where flexible performance within 2 sec was confirmed.

Table 6. Online OET Test.

Test	Input	Time/Result		Judgment
Online OET Test	Measuring by adjusting the generator field current	IF: 2.0 PU	TRIP	Approx. 2 s/Confirmed Pass

6.2. Analog Input Test

A test was performed to check the integrity during signal processing for the analog signal of KDR-1200D prior to starting the generator. The test items and conditions were as follows:

For the test, the line outputting to the generator field coil was opened for the safety of the test and protection. The PT and CT cables leading to the AVR panel were then detached. Moreover, by using the PT/CT simulator, a connection was established to impress the current signal. Measurements of generator voltage, reactive power, and active power were taken by applying the PT (CT) voltage to PT (CT). Meanwhile, values of reactive and active power were recorded by shifting the generator current 45° each time. Finally, after recording the values of generator voltage, frequency, and reactive/active power, the PT and CT cables were restored.

The test items at the rated generator voltage/current/frequency are shown in Table 7. Several precautions were taken. In the CT test, we checked with DMM or others in advance to make sure that the CT was not in open state and confirmed that frequency detection was performed at or over 5% of the rated generator voltage.

Table 7. Test Items at the Rated Generator Voltage/Current/Frequency.

Test Items	Criteria	Result		Judgment
		MASTER	BACKUP	
		KDR-1200D	KDR-1200D	
P	Lead Phase 90°	0.0000	0.0012	Pass
	Lead Phase 45°	0.7070	0.7080	
	In Phase	1.0000	0.9998	
	Lag Phase 45°	0.7070	0.7063	
	Lag Phase 90°	0.0000	0.0000	
Q	Lead Phase 90°	-1.0000	-1.0000	Pass
	Lead Phase 45°	-0.7070	-0.7064	
	In Phase	0.0000	0.0000	
	Lag Phase 45°	0.7070	0.7081	
	Lag Phase 90°	1.0000	1.0000	

* Caution: Check with DMM or others in advance to make sure that CT is not in open state; Frequency detection should be performed at or over 5% of the rated generator voltage.

The test items for PT variant generator terminal voltage are shown in Table 8, and those for variant VF and variant VF, PCR1 and PCR2 IF are listed in Tables 9 and 10, respectively. Meanwhile, the test items for the ETF PT/CT input test are presented in Table 11.

Table 8. PT Variant Generator Terminal Voltage.

Test Items	Criteria	Result		Judgment
		Master	Backup	
Vrms	16.6 V	0.25 PU	0.0000	0.0000
	33.2 V	0.50 PU	0.4964	0.4966
	66.39 V	1.00 PU	0.9999	1.0000
	83 V	1.25 PU	1.2019	1.2018
Hz	48 Hz	0.80 PU	0.8003	0.8000
	54 Hz	0.90 PU	0.9000	0.9001
	60 Hz	1.00 PU	1.0001	1.0001
	66 Hz	1.10 PU	1.1001	1.1000

Table 9. VF, PCR1 and PCR2.

Test Items	Criteria	Result		Judgment
		Master	Backup	
VF	Take measurement by changing the field Voltage IF (VF Rated = 82 V)	0 V/0.0 V	0.000 PU	0.0001 0.0000
		2.733 V	0.500 PU	0.4999 0.4999
		5.466 V	1.000 PU	1.0000 1.0000
		8.199 V	1.500 PU	1.5000 1.4999

Table 10. IF, PCR1 and PCR2.

Test Items	Criteria	Result		Judgment
		Master	Backup	
IF	Take measurement by changing the field current IF (IF Rated = 23 A) [4.6 V/23 A]	0 V	0.00 PU	0.0000 0.0000
		2.3 V	0.50 PU	0.4985 0.4986
		4.6 V	1.00 PU	0.9999 0.9998
		6.9 V	1.50 PU	1.4970 1.4953
PCR1_IF	Take measurement by changing the PCR1 current (IF Rated = 23 A) [4.6 V/23 A]	9.2 V	2.00 PU	1.9963 1.9944
		0 V	0.00 PU	0.0000 0.0000
		2.3 V	0.50 PU	0.4987 0.4983
		4.6 V	1.00 PU	1.0000 1.0000
PCR2_IF	Take measurement by changing the PCR2 current (IF Rated = 23 A) [4.6 V/23 A]	6.9 V	1.50 PU	1.4980 1.4963
		9.2 V	2.00 PU	1.9949 1.9950
		0 V	0.00 PU	0.0000 0.0000
		2.3 V	0.50 PU	0.4965 0.4947

Table 11. ETF PT/CT Input Test.

Classification	Ratio	ETP Input (Main)	ETP Input (Measure)	Remarks
Rated Generator Voltage	13,800 V/115 V	A: 4.953 V; B: 4.764 V; C: 4.979 V	A: 4.626 V; B: 4.967 V; C: 5.038 V	-
Rated Generator Current	4987 A/4.156 A	4.081 V	-	-

6.3. Analog Output Test

A test was performed to check the integrity during signal processing for the analog output signal of KDR-1200D prior to starting the generator. The test items and conditions are shown in Table 12. The test items are shown in Tables 13 and 14, and the Test Bed worked flexibly. We set a Test Mode at TOP of KDR-1200D, and then applied the test mode input signals (0–2.0 PU) to record the actual analog output values with a DMM. Finally, we applied the rated voltage and current to check and record the actual output signal and Real Value on the TOP screen.

Table 12. Test Items and Conditions.

Channel No.	Channel Name	Channel No.	Channel Name
AO-1	Con_Signal1	AO-5	AO_VT
AO-2	Con_Signal2	AO-6	AO_FREQ/AO_P(MW)
AO-3	AO_IF	AO-7	AO_Q(Mvar)
AO-4	Balance_Meter	AO-8	AO_Con_Signal

Table 13. Test Items Worked Flexibly (1).

	Test Items	Criteria		Master	Backup	Judgment
		[Card1]	[Card1]	[Card1]	[Card1]	
AO1	Take measurement by changing the PCR firing control signals (0–10 V)	0.0 PU	0.00 V ($\pm 5\%$)	-0.011	-0.024	Pass
		0.5 PU	2.50 V ($\pm 5\%$)	2.461	2.448	
		1.0 PU	5.00 V ($\pm 5\%$)	4.939	4.927	
		1.5 PU	7.50 V ($\pm 5\%$)	7.42	7.41	
		2.0 PU	10.00 V ($\pm 5\%$)	9.89	9.88	

Table 14. Test Items Worked Flexibly (2).

	Test Items	Criteria		Master	Backup	Judgment
		[Card1]	[Card1]	[Card1]	[Card1]	
AO2	Take measurement by changing the PCR firing control signals (0–10 V)	0.0 PU	0.00 V ($\pm 5\%$)	-0.035	-0.033	Pass
		0.5 PU	2.50 V ($\pm 5\%$)	2.432	2.430	
		1.0 PU	5.00 V ($\pm 5\%$)	4.905	4.898	
		1.5 PU	7.50 V ($\pm 5\%$)	7.38	7.37	
		2.0 PU	10.00 V ($\pm 5\%$)	9.85	9.83	

7. Conclusions

The excitation system is a crucial system for various types of power plants as well as the smart factories of the 4th Industrial Revolution. It maintains or controls the output terminal voltage by supplying direct current to the field winding. It is part of the internal system of an emergency diesel generator, generating voltage for the generator and supplying constant current to various types of equipment uniformly. As a core piece of equipment that supplies power to the cooling pump or cooling fan necessary for the cooling of nuclear reactors or other power-generating facilities, the emergency diesel generator is activated as soon as these facilities stop. The excitation system assumes the role of assisting the emergency diesel generator in maintaining constant voltage and running properly by comprehensively controlling the currents. It automatically kicks in when the nuclear reactor or power generation facility stops operating and restores power in the power plant within 10 s. Even if the voltage of the emergency diesel generator drops suddenly, the system will restore it to the original level. Ultimately, the excitation system is a core piece of equipment that allows the emergency diesel generator, cooling facility, or nuclear reactor to work properly in an emergency that causes failure. The excitation systems currently used by most of the power stations in the Republic of Korea were installed during the 1970s or 1980s. Unfortunately, it is difficult to seek technical assistance for them as they depend on foreign technologies, requiring a large sum to be paid when requesting one or more engineers to be dispatched. As such, technical updates have always been made by foreign companies, since it is not easy to make modifications to the system without the help of the original system developer. The technology developed in this study was designed to address such problem. The inability to conduct a test for an actual system can be solved by using a power system analysis program to analyze the characteristics of the controller. Thus, in this study, a field test was conducted on the test bed to optimize a redundant digital excitation system. The integrity of the proposed framework

was confirmed by conducting a comprehensive performance test, for which a number of international standards including IEEE were adopted. At the same time, a series of simulations was conducted for the framework using a power system analysis ETAP Simulation. For the redundant controller, abnormal operation or functional failures were determined by the relay board. The integrity of the controller was then tested through the generation of periodic signals by embedding a surveillance timer within the controller. Thus, by designing the system in such a way as to avoid a “Voltage droop” at the time of controller switchover, the stability of the entire power system could be guaranteed.

After identifying/confirming the response characteristics of the excitation system through simulations, and with the support of a protective relay, the stability of the entire power system can be maintained even in case of an actual accident in the power plant.

The response characteristics of the excitation system will be investigated with the proposed simulation model; to support power system operation in case of an accident, collaborative work will be performed with the protective relay.

For the start control of a 37 kW DC motor, which supplies emergency power to the major facilities of a power station, simulations were performed with the PSIM program. The result of the simulations satisfied the condition wherein the initial start current should be operated within 200% of the rated normal current of 170 amp.

Such DC motor start system is expected to make a significant contribution to the operational stability of power stations. This study also presented a new technique for improving the excitation system’s start features. Compared to the existing analog system, which takes about 9.88 s to start with a timer, the proposed system started the motor within 4.88 s by measuring the slip; it was also more efficient since it shortened the delay. This method is also expected to contribute to the stability of excitation systems since it can guarantee stable startup by initially preventing the DC field current from being supplied at a faster rate than the synchronous speed through the measurement of the rotor slip. The redundant digital excitation system proposed in this study is expected to increase both the stability and economic effectiveness of a system by optimizing existing systems.

In the future, the authors plan to focus on student education by establishing an education system that allows students to learn about the digital excitation system and its simulation.

Author Contributions: Conceptualization, J.-H.H.; Data curation, H.-G.L.; Formal analysis, J.-H.H.; Funding acquisition, J.-H.H.; Methodology, H.-G.L.; Project administration, J.-H.H.; Resources, H.-G.L.; Software, J.-H.H.; Supervision, H.-G.L.; Validation, H.-G.L.; Visualization, H.-G.L.; Writing—original draft, J.-H.H. and H.-G.L.; Writing—review and editing, J.-H.H. and H.-G.L.

Funding: This work was supported by the National Research Foundation of Korea (NRF) grant funded by the Korea government (MSIT) (No. 2017R1C1B5077157).

Conflicts of Interest: The authors declare no conflict of interest.

Abbreviations

ADC	Analog-Digital Converter
AVR	Auto Voltage Regulator
CPU	Central Processing Unit
DC	Direct Current
DFT	Discrete Fourier Transform
DSP	Digital Signal Process
ETAP	Electrical Transient Analyzer Program
FCR	Field Current Regulator
FPGA	Field-Programmable Gate Array
HMI	Human-Machine Interface
ICT	Information and Communications Technologies
IEEE	Institute of Electrical and Electronics Engineers
IGBT	Insulated Gate Bipolar Transistor

KEPCO	Korea Electric Power Corporation's
MVR	Manual Voltage Regulator
OEL	Over Excitation Limit
OET	Over Excitation Trip
OS	Operating System
PID	Proportional Integral Derivative
PT	Potential Transformer
PSIM	Powersim inc.
PWM	Pulse Width Modulation
RPM	Revolution Per Minute
RTOS	Real-Time Operating System
UEL	Under Excitation Limit
TMR	Triple Modular Redundant
VSC	Voltage Source Converter
SMES	Superconducting Magnetic Energy Storage

References

1. Ramakrishnan, K. Delay-Dependent Stability of Networked Generator-Excitation Control Systems: An LMI based Approach. *IFAC-PapersOnLine* **2016**, *49*, 431–436. [[CrossRef](#)]
2. Aldeen, M.; Saha, S.; Evans, R.J. Faults detection and mitigation in excitation control of synchronous machines in large-scale power grids. In Proceedings of the 8th IEEE GCC Conference and Exhibition, Muscat, Oman, 1–4 February 2015.
3. Liu, Z.; Yao, W.; Wen, J. Enhancement of Power System Stability Using a Novel Power System Stabilizer with Large Critical Gain. *Energies* **2017**, *10*, 449. [[CrossRef](#)]
4. Schimpe, M.; Piesch, C.; Hesse, H.C.; Paß, J.; Ritter, S.; Jossen, A. Power Flow Distribution Strategy for Improved Power Electronics Energy Efficiency in Battery Storage Systems: Development and Implementation in a Utility-Scale System. *Energies* **2018**, *11*, 533. [[CrossRef](#)]
5. Huh, J.-H. PLC-Integrated Sensing Technology in Mountain Regions for Drone Landing Sites: Focusing on Software Technology. *Sensors* **2018**, *18*, 2693. [[CrossRef](#)] [[PubMed](#)]
6. Liu, J.; Miura, Y.; Bevrani, H.; Ise, T. Enhanced Virtual Synchronous Generator Control for Parallel Inverters in Microgrids. *IEEE Trans. Smart Grid* **2017**, *8*, 2268–2277. [[CrossRef](#)]
7. Lee, H.G.; Huh, J.H. A Cost-Effective Redundant Digital Excitation Control System and Test Bed Experiment for Safe Power Supply for Process Industry 4.0. *Processes* **2018**, *6*, 85. [[CrossRef](#)]
8. Yang, L.; Wang, J.; Ma, Y.; Wang, J.; Zhang, X.; Tolbert, L.M.; Wang, F.F.; Tomsovic, K. Three-Phase Power Converter-based Real-Time Synchronous Generator Emulation. *IEEE Trans. Power Electron.* **2017**, *32*, 1651–1665. [[CrossRef](#)]
9. Deng, Y.; Zhou, B.; Xing, C.; Zhang, R. Multifrequency Excitation Method for Rapid and Accurate Dynamic Test of Micromachined Gyroscope Chips. *Sensors* **2014**, *14*, 19507–19516. [[CrossRef](#)] [[PubMed](#)]
10. Fraga-Lamas, P.; Noceda-Davila, D.; Fernández-Caramés, T.M.; Díaz-Bouza, M.A.; Vilar-Montesinos, M. Smart Pipe System for a Shipyard 4.0. *Sensors* **2016**, *16*, 2186. [[CrossRef](#)] [[PubMed](#)]
11. Ryu, H.S.; Kim, S.Y.; Kim, J.M.; Lim, L.H. Denelopment of Generator Excitation System with Main/siandby Controller in Inchun Thermal Power Plant #4. *TKPE* **1999**, *4*, 507–514.
12. Kim, G.; Lim, I. A Study on the Development and the Application of Redundant Digital Excitation System for the Power Plants. *J. KIIE* **2001**, *15*, 97–107.
13. Chae-Ho, N.; Nam, J.H.; Choi, J.H.; Baeg, S.Y.; Cho, C.H. Design and Implementation of a Duplex Digital Excitation Control System for Power Plants. In Proceedings of the International Conference on Control, Automation and Systems, Jeju Island, Korea, 17–21 October 2001; pp. 2383–2386.
14. Ryu, H.S.; Shin, M.S.; Lee, J.H.; Lim, I.H. A Study of Digital Excitation System for Pumped Storage Power Plant. In Proceedings of the KIEE Conference, Seoul, Korea, 10–12 July 2002; pp. 1018–1020.
15. Lee, J.D.; Lim, I.H.; Lee, J.H.; Ryu, H.S.; Shin, M.S. Analysis for Digital Excitation System with IGBT Devices. In Proceedings of the KIEE Conference, Seoul, Korea, 21–23 July 2003; pp. 1105–1107.

16. Jang, S.J.; Ryu, D.K.; Seo, M.S.; Kim, J.H.; Won, C.W.; Lee, J.K. A Study on Excitation System for Synchronous Generator using Current Mode Controlled PWM Converter. *J. Korean Inst. Illum. Electr. Install. Eng.* **2003**, *17*, 32–39.
17. Ryu, H.S.; Shin, M.S.; Lee, J.H.; Lim, I.H. A Study of Simulator for Static Digital Excitation System. In Proceedings of the TKPE, Muju, Korea, 11 July 2005; pp. 162–165.
18. Shin, M.S.; Ryu, H.S.; Lee, J.H.; Lim, I.H.; Kim, B.S.; Song, S.I. The Development of Control & Diagnostic Technique for Digital Excitation System. In Proceedings of the KIEE, Seoul, Korea, 18–20 July 2005; pp. 2597–2599.
19. Ryu, H.S.; Shin, M.S.; Lee, J.H.; Lim, I.H. The Development of Redundant Excitation System for Sudan Khartoum Power Plant. In Proceedings of the KIPE, Gyeongju, Korea, 7 July 2009; pp. 24–26.
20. Lee, J.H.; Lim, I.H.; Shin, M.S.; Jeong, T.W. The Development of Digital Excitation Control System for Diesel Generator of Nuclear Power Plant and Its Application. *J. KIEE* **2010**, *59*, 1449–1455.
21. Ryu, H.S.; Lee, J.H.; Lim, I.H. A Study on the Dual PWM Digital Excitation System of Regeneration Type. *J. Korean Inst. Illum. Electr. Install. Eng.* **2010**, *24*, 79–84. [[CrossRef](#)]
22. Jun, S. Application of Thyristor Dynamic Stability Test for Digital Excitation System. In Proceedings of the KIEE, Seoul, Korea, 21–23 October 2010; pp. 131–133.
23. Ryu, H.S.; Shin, M.S.; Lee, J.H.; Lim, I.H. A Study of Function Verification of Digital Excitation System with Real Time Simulator. In Proceedings of the KIEE, Seoul, Korea, 20–22 July 2011; pp. 1191–1192.
24. Ryu, H.S.; Cha, H. Development of the Triple Modular Redundant Excitation System with Simulator for 500MW Synchronous Generator. *Trans. Korean Inst. Electr. Eng.* **2014**, *63*, 70–75. [[CrossRef](#)]
25. Máslo, K.; Kasembe, A.; Kolcun, M. Simplification and unification of IEEE standard models for excitation systems. *Electr. Power Syst. Res.* **2016**, *140*, 132–138. [[CrossRef](#)]
26. Yousef, H.; Soliman, H.M.; Albadi, M. Nonlinear power system excitation control using adaptive wavelet networks. *Neurocomputing* **2017**, *230*, 302–311. [[CrossRef](#)]
27. Yang, J.; Chen, Z.; Mao, C.; Wang, D.; Lu, J.; Sun, J.; Li, M.; Li, D.; Li, X. Analusis and Assessment of VSC Excitation System for Power System Stability Enhancement. *Electr. Power Energy Syst.* **2014**, *57*, 350–357. [[CrossRef](#)]
28. Aldeen, M.; Saha, S. Decentralised fault detection, identification, and mitigation in excitation control systems. *Electr. Power Energy Syst.* **2016**, *77*, 302–313. [[CrossRef](#)]
29. Zhang, H.; Hu, B. The Application of Nonlinear PID Controller in Generator Excitation System. In Proceedings of the 2012 International Conference on Future Electrical Power and Energy Systems Energy Procedia, Sanya, China, 21–22 February 2012; Volume 17, pp. 202–207.
30. Saavedra-Montes, A.J.; Ramirez-Scarpetta, J.M.; Ramos-Paja, C.A.; Malik, O.P. Identification of excitation system with the generator online. *Electr. Power Syst. Res.* **2012**, *87*, 1–9. [[CrossRef](#)]
31. Saavedra-Montes, A.J.; Ramirez-Scarpetta, J.M.; Malik, O.P. Methodology to estimate parameters of an excitation system based on experimental conditions. *Electr. Power Syst. Res.* **2011**, *81*, 170–176. [[CrossRef](#)]
32. Khodabakhshian, A.; Morshed, M.J.; Parastegari, M. Coordinated design of STATCOM and excitation system controllers for multi-machine power systems using zero dynamics method. *Electr. Power Energy Syst.* **2013**, *49*, 269–279. [[CrossRef](#)]
33. Berube, G.R.; Hajagos, L.M.; Beaulieu, R.E. A Utility Perspective on Under-Excitation Limiters. *IEEE Trans. Energy Convers.* **1995**, *10*, 532–537. [[CrossRef](#)]
34. Freitas, W.; Vieira, J.C.; Morelato, A.; Xu, W. Influence of Excitation System Control Modes on the Allowable Penetration Level of Distributed Synchronous Generators. *IEEE Trans. Energy Convers.* **2005**, *20*, 474–480. [[CrossRef](#)]
35. Hurley, J.D.; Bize, L.N.; Mummert, C.R. The Adverse Effects of Excitation System Var and Power Factor Coontrollers. *IEEE Trans. Energy Convers.* **1999**, *14*, 1636–1645. [[CrossRef](#)]
36. Shi, J.; Tang, Y.; Xia, Y.; Ren, L.; Li, J. SMES Based Excitation System for Doubly-Fed Induction Generator in Wind Power Application. *IEEE Trans. Appl. Supercond.* **2011**, *21*, 1105–1108. [[CrossRef](#)]
37. Zhang, X.C.; Cheng, G.H.; Xu, Z. Transmission and User Defined Excitation System Models for Power System Stability Analysis in PSASP. In Proceedings of the Transmission and Distribution Conference and Exhibition: Asia and Pacific, Dalian, China, 18 August 2005; pp. 1–5.
38. Dandeno, P.L.; Karas, A.N.; McClymont, K.R.; Watson, W. Effect of High-Speed Rectifier Excitation Systems on Generator Stability Limits. *IEEE Trans. Power App. Syst.* **1968**, *87*, 190–201. [[CrossRef](#)]

39. Wang, D.; Mao, C.; Lu, J. Coordinated Control of EPT and Generator Excitation System for Multidouble-Circuit Transmission-Lines System. *IEEE Trans. Power Deliv.* **2008**, *23*, 371–379. [[CrossRef](#)]
40. Huh, J.-H. Smart Grid Test Bed Using OPNET and Power Line Communication. In *Advances in Computer and Electrical Engineering*; IGI Global: Hershey, PA, USA, 2017; pp. 64–89.



© 2018 by the authors. Licensee MDPI, Basel, Switzerland. This article is an open access article distributed under the terms and conditions of the Creative Commons Attribution (CC BY) license (<http://creativecommons.org/licenses/by/4.0/>).